

THE GALAXY–HALO/SUBHALO CONNECTION: MASS RELATIONS AND IMPLICATIONS FOR SOME SATELLITE OCCUPATIONAL DISTRIBUTIONS

A. RODRÍGUEZ-PUEBLA, V. AVILA-REESE AND N. DRORY

Instituto de Astronomía, Universidad Nacional Autónoma de México, A. P. 70-264, 04510, México, D.F., México.

Submitted to ApJ

ABSTRACT

We infer the local stellar-to-halo/subhalo mass relations (MRs) for central and satellite galaxies *separately*. Our statistical method is extending the abundance matching, halo occupation distribution, and conditional stellar mass function formalisms. We constrain the model using several combinations of observational data, consisting of the total galaxy stellar mass function (GSMF), its decomposition into centrals and satellites, and the projected two-point correlation functions (2PCFs) measured in different stellar mass (M_*) bins. In addition, we use the Λ CDM halo and subhalo mass functions. The differences among the resulting MRs are within the model-fit uncertainties (which are very small, smaller than the intrinsic scatter between galaxy and halo mass), no matter what combination of data are used. This shows that matching abundances or occupational numbers is equivalent, and that the GSMFs and 2PCFs are tightly connected. We also constrain the values of the intrinsic scatter around the central-halo (CH) and satellite-subhalo (SS) MRs assuming them to be constant: $\sigma_c = 0.168 \pm 0.051$ dex and $\sigma_s = 0.172 \pm 0.057$ dex, respectively. The CH and SS MRs are actually different, in particular when we take the subhalo mass at the present-day epoch instead of at their accretion time. When using the MRs for studying the satellite population (e.g., in the Milky Way, MW), the SS MR should be chosen instead of the average one. Our model allows one to calculate several population statistics. We find that the central galaxy M_* is not on average within the mass distribution of the most-massive satellite, even for cluster-sized halos, i.e., centrals are not a mere realization of the high-end of the satellite mass function; however for $> 3 \times 10^{13} M_\odot$ halos, $\sim 15\%$ of centrals could be. We also find that the probabilities of MW-sized halos of having N Magellanic-Clouds (MCs)-sized satellites agree well with observational measures; for a halo mass of $2 \times 10^{12} M_\odot$, the probability to have 2 MCs is 5.4%, but if we exclude those systems with satellites larger than the MCs, then the probability decreases to $< 2.2\%$.

Subject headings: galaxies: abundances — galaxies: evolution — galaxies: halos — galaxies: luminosity function, mass function — galaxies: statistics — cosmology: dark matter.

1. INTRODUCTION

The statistical description of the galaxy population is a valuable tool for understanding the properties of galaxies and the way they cluster, as well as the role that mass and environment play in shaping these properties. Moreover, statistical descriptors such as the luminosity function, the galaxy stellar mass function (GSMF), and the two-point correlation function (2PCF) has allowed us to probe galaxy evolution and its connection to the cosmological initial conditions of structure formation (e.g., Peebles 1980; Yoo et al. 2009). Such a connection is of vital importance in studies devoted to the development of the current Λ CDM cosmological paradigm. A key ingredient in these studies is the link between galaxy and dark matter halo properties. Such a link allows to project the theoretical dark matter halo population onto the observable galaxies.

Recently, progress towards connecting galaxies and halos has been made through the development of several techniques for observationally estimating the dark halo masses of luminous galaxies, such as weak lensing (Mandelbaum et al. 2006; Mandelbaum, Seljak & Hirata 2008; Schulz, Mandelbaum & Padmanabhan 2010), kinematics of satellite galaxies (Conroy et al. 2007; More et al.

2009, 2011; Wojtak & Mamon 2013), and galaxy clusters (Yang et al. 2007; Yang, Mo & van den Bosch 2009a; Hansen et al. 2009; Yang et al. 2012). However, these direct probes of halo mass still have large uncertainties.

Consequentially, semi-empirical approaches that link the galaxy and dark matter halo distributions statistically are of great importance. For example, the Halo Occupation Distribution (HOD) formalism, which describes the probability for finding N galaxies in halos of mass M_h , has been used successfully to understand the non-linear relation between the distribution of galaxies and matter, for instance, at the level of the power spectra (Seljak 2000; Peacock & Smith 2000; Cooray & Sheth 2002; Yoo et al. 2009), or the two-point correlation functions (Berlind & Weinberg 2002; Cooray & Sheth 2002; Zehavi et al. 2005; Abbas & Sheth 2006; Tinker et al. 2008b; Zehavi et al. 2011; Watson, Berlind & Zentner 2011; Watson et al. 2012; Wake, Franx & van Dokkum 2012, and references therein).

However, the HOD model provides only information on the total number of galaxies above some luminosity or stellar mass threshold per halo, and constrains only the halo mass of the central galaxy. In order to describe the detailed halo occupation and mass distribution of central and satellite galaxies, Yang, Mo & van den Bosch (2003) introduced the conditional luminosity (or stellar mass) function (CSMF) in the HOD model (see

also e.g., Yang, Mo & van den Bosch 2009a, hereafter YMB09, Moster et al. 2010; Leauthaud et al. 2011, 2012; Yang et al. 2012). The CSMF is defined as the average number of galaxies with stellar masses between $M_* \pm dM_*/2$ occupying a halo of a given mass M_h . Nevertheless, both the HOD model and the CSMF formalism assume a parametric description for the satellite population distributions which is constrained using observations.

In order to avoid an arbitrary parametric description for the satellite population, the above models can be generalized with the abundance matching technique (hereafter, AMT; e.g., Vale & Ostriker 2004; Kravtsov et al. 2004; Conroy, Wechsler & Kravtsov 2006; Shankar et al. 2006; Weinberg et al. 2008; Baldry, Glazebrook & Driver 2008; Conroy & Wechsler 2009; Drory et al. 2009; Moster et al. 2010; Behroozi, Conroy & Wechsler 2010; Guo et al. 2010; Behroozi, Wechsler & Conroy 2012; Reddick et al. 2012; Papastergis et al. 2012). Under the hypothesis that there exists a one-to-one monotonic relation between stellar mass and (sub)halo mass, the matching the total galaxy and halo plus subhalo abundances yields a *global* (average) relation between M_* and M_h . Note that in this simple procedure, the central-to-halo and satellite-to-subhalo mass relations (hereafter CHMR and SSMR, respectively) are not differentiated. Recently, Simha et al. (2012) have found in their cosmological N-body/hydrodynamics simulations that both mass relations are nearly identical if the subhalo masses, m_{sub} , are defined at their accretion times. Additionally, previous studies have shown that when the AMT results are applied to the HOD model with m_{sub} defined at the accretion epoch, then the spatial clustering of galaxies is mostly recovered (e.g., Conroy, Wechsler & Kravtsov 2006; Moster et al. 2010). Similar results are expected when m_{sub} is defined at the observation time but a global offset is applied to account for the average effect of subhalo mass loss due to tidal stripping (Vale & Ostriker 2004; Weinberg et al. 2008).

On the other hand, there is no reason to assume a priori the SSMR to be identical to the CHMR (Neistein et al. 2011, Rodríguez-Puebla, Drory & Avila-Reese 2012, hereafter RDA12). For accretion-time m_{sub} , such an assumption implies that the change of the stellar masses of satellites after their accretion will be such that they would occupy the $z = 0$ central-to-halo mass relation or, more generally, that the CHMR almost does not change with time. Recent studies based on large halo-based group catalogs (e.g., Wetzel, Tinker & Conroy 2012) or on the predicted bulge-to-total mass ratio of central galaxies (Zavala et al. 2012) have shown that once satellite galaxies are accreted, they evolve roughly as a central galaxy at least for several Gyrs. This could imply that the SSMR with m_{sub} defined at accretion time may not be equal to the $z = 0$ CHMR. Nevertheless, in the cosmological simulations of Simha et al. (2012), despite the fact that satellites continue to grow after accretion, both mass relations end up similar. It is therefore likely that the growth in mass as well as the change of the CHMR with time are very small.

In RDA12 we extended the AMT to determine the CHMR and SSMR separately, using the observed decomposition of the GSMFs into centrals and satellites. We

have found that indeed the SSMR is not equal to the CHMR, and that applying them to the HOD + CSMF model leads to satellite CSMF and correlation functions in excellent agreement with observational data. Actually, when m_{sub} is defined at the accretion time, the $z = 0$ mass relations become close but not equal (see Fig. 2 in RDA12). Additionally, RDA12 show that the uncertainty in the AMT related to the satellite stellar mass growth can be avoided if subhalo masses are defined at the time of observation rather than at the time of accretion. RDA12 also suggest that the central-halo and satellite-subhalo mass relations can be determined simultaneously using the correlation functions as observational input, instead of the GSMF decomposed into satellites and centrals. This is presumably because *matching abundances of satellite to subhalos is essentially equivalent to matching their corresponding occupational numbers (and vice versa)*.

In the present paper, we aim to test the above statements. We will also probe how robust the determinations of the central-to-halo and satellite-to-subhalo mass relations through our extended AMT and HOD+CSMF combined model are. We will explore whether these mass relations vary significantly depending on the combinations of observational data being used; in particular, we will explore whether the uncertainties in the model parameters that describe the mass relations shrink significantly when more observational constraints are added.

Our model proves to be a powerful tool for connecting the Λ CDM (sub)halo statistics to the statistics of the central/satellite galaxy populations. In this sense, one may predict many halo occupational distributions and probabilities as a function of scale; for instance, the mass distribution of the most massive satellites as a function of halo mass or the probability of a halo hosting N satellites in a given stellar mass range or, more generally, the whole satellite CSMF. We will discuss some results obtained for these occupational distributions and probabilities.

In Section 2 we describe our extended AMT and HOD+CSMF model, and present the different combinations of data to be used to constrain the model parameters. The results of our model for the different data sets are presented in Section 3. In particular, we compare the central-halo and satellite-subhalo mass relations obtained using different data sets. We also constrain the intrinsic scatter around the mean central-halo and satellite-subhalo mass relations. In §4 we discuss the halo occupational statistics related to the halo mass dependence of the satellite CSMF, the stellar mass gap between the most massive satellite and the central galaxy, and the probabilities of Milky-Way (MW) sized halos having 1, 2, or more Magellanic Cloud-sized satellites. Section 5 is devoted to discuss the robustness of the obtained mass relations and their model uncertainties, as well as the implications of extrapolating our obtained SSMR to masses as small as the MW dwarf spheroidal galaxies. Finally, we present our conclusions in Section 6.

We adopt cosmological parameter values close to WMAP 7: $\Omega_\Lambda = 0.73$, $\Omega_M = 0.27$, $h = 0.70$, $n_s = 0.98$ and $\sigma_8 = 0.84$.

2. METHODOLOGY

In the following we present our model connecting galaxies to halos and subhalos via their occupational

numbers. This is done under the assumption that on average the central-to-halo and satellite-to-subhalo relations are monotonic. The model relates in a self-consistent way the GSMF decomposed into centrals and satellites, the Λ CDM halo/subhalo mass functions, the satellite CSMFs, and the galaxy projected 2PCFs. As a result, it constrains both the CHMR and the SSMR, and predicts the satellite CSMF and several other occupational statistics. Unlike previous models of this kind (e.g., Moster et al. 2010), the CHMR and SSMR are treated separately.

2.1. Connecting galaxies to halos and subhalos

The *total* GSMF is decomposed into satellites and central galaxies,

$$\phi_g(M_*) = \phi_{g,\text{cen}}(M_*) + \phi_{g,\text{sat}}(M_*), \quad (1)$$

which after integration yields the mean cumulative number density of galaxies with stellar masses greater than M_* ,

$$\int_{M_*}^{\infty} \phi_g dM_*' = \int_{M_*}^{\infty} \phi_{g,\text{cen}} dM_*' + \int_{M_*}^{\infty} \phi_{g,\text{sat}} dM_*', \quad (2)$$

or, in short,

$$n_g(> M_*) = n_{g,\text{cen}}(> M_*) + n_{g,\text{sat}}(> M_*). \quad (3)$$

2.1.1. Central galaxies

For constructing the central GSMF, we will use the conditional probability that a given halo of mass M_h is inhabited by a central galaxy with stellar mass between $M_* \pm dM_*/2$, $P_{\text{cen}}(M_*|M_h)dM_*$, and assume this distribution to be log-normal:

$$P_{\text{cen}}(M_*|M_h)dM_* = \frac{dM_*}{\sqrt{2\pi\sigma_c^2 M_*} \ln(10)} \times \exp\left[-\frac{\log^2(M_*/M_{*,c}(M_h))}{2\sigma_c^2}\right], \quad (4)$$

with σ_c being the intrinsic scatter (width), expressed in dex units, around $\log M_{*,c}(M_h)$, the mean stellar-to-halo mass relation of *central galaxies* (CHMR). Formally, $P_{\text{cen}}(M_*|M_h)$ maps the halo mass function, HMF, onto the central GSMF, thereby encoding all the physical processes involved in galaxy formation inside the halos. We parametrize $\log M_{*,c}(M_h)$ using the functional form proposed by Behroozi, Wechsler & Conroy (2012),

$$\log M_{*,c}(M_h) = \log(\epsilon_c M_{1,c}) + f(\log(M_h/M_{1,c})) - f(0\bar{h})$$

where

$$f(x) = \delta_c \frac{(\log(1 + e^x))^{\gamma_c}}{1 + e^{10^{-x}}} - \log(10^{\alpha_c x} + 1). \quad (6)$$

This function behaves as power law with slope α at masses much smaller than $M_{1,c}$, and as a sub-power law with slope γ_c at larger masses. This parametrization maps the Λ CDM HMF to a Schechter-like GSMF (Schechter 1976).

The mean number density of central galaxies with stellar masses between $M_* \pm dM_*/2$, (i.e., the central GSMF)

is given by

$$\phi_{g,\text{cen}}(M_*)dM_* = dM_* \int_0^{\infty} P_{\text{cen}}(M_*|M_h)\phi_h(M_h)dM_h, \quad (7)$$

where $\phi_h(M_h)$ is the *distinct* HMF. We use the fitted results to the *distinct* HMF from cosmological simulations carried out in Tinker et al. (2008a) as reported in their Appendix B. Here we define halo masses at the virial radius, i.e. the halo radius where the spherical overdensity is Δ_{vir} times the mean matter density, with $\Delta_{\text{vir}} = (18\pi^2 + 82x - 39x^2)/\Omega(z)$, and $\Omega(z) = \rho_m(z)/\rho_{\text{crit}}$ and $x = \Omega(z) - 1$ (Bryan & Norman 1998).

Having defined $P_{\text{cen}}(M_*|M_h)$, the cumulative probability that a halo of mass M_h hosts a central galaxy with a stellar mass greater than M_* is simply

$$\int_{M_*}^{\infty} P_{\text{cen}}(M_*|M_h)dM_*, \quad (8)$$

which coincides with the definition of the mean occupational number of central galaxies, $\langle N_c(> M_*|M_h) \rangle$. Finally, we are able to infer the mean number density of galaxies with stellar mass greater than M_* , that is, $n_{g,\text{cen}}(> M_*) = \int_0^{\infty} \langle N_c(> M_*|M_h) \rangle \phi_h(M_h) dM_h$.

2.1.2. Satellite galaxies

Since satellites are expected to reside in subhalos, we will use a similar approach to centrals, i.e. we will establish a link between the properties of satellite galaxies to those of the subhalos. However, in this case, one should take into account that (i) before becoming a satellite they occupy a distinct halo, and (ii) the subhalo mass, m_{sub} , can be defined at the observation time (their present-day mass in our case) or at the accretion time (the epoch when a distinct halo became a subhalo).

Item (ii) is discussed in RDA12. First, RDA12 show that once the subhalo mass function is provided for any definition of subhalo mass, the satellite-to-subhalo mass relation, SSMR, can be constrained consistently with the observed satellite GSMF. Therefore, the use of one or another is subject to practical criteria. On one hand, with the accretion-epoch definition, the central and satellite mass relations are almost the same, as observations (RDA12) and simulations (Simha et al. 2012) show, and the obtained SSMR for this case is free of a potential dependence on host halo mass. Besides, the accretion-time m_{sub} definition is less sensitive to the specifics of the halo finding algorithm than the observed-time definition. On the other hand, the SSMR for the subhalo mass defined at accretion time is actually a nominal relation, where the abundance matching is carried out for the satellite GSMF at the *present epoch* but for a subhalo mass function constructed for subhalos accreted at *different previous epochs*. The physical interpretation of this nominal relation requires assumptions about the evolution of galaxies. Instead, when matching present-day satellite abundances with present-day subhalo abundances, the connection is direct and no assumptions about evolution are necessary (see RDA12, §§4.1, for an extensive discussion).

Here, our constraints for the SSMR refer to m_{sub} defined at the same epoch that the observational input is

provided for, that is the present time. However, some results will be presented also for the accretion-time m_{sub} .

For the subhalo abundance, given as the subhalo conditional mass function, we use the results obtained in Boylan-Kolchin et al. (2010) based on the Millennium-II simulation. It is worth noting that the lowest subhalo masses we probe in this work ($\sim 10^{10} - 10^{11} M_{\odot}$, depending on the GSMF used) are around 3–4 orders of magnitude above the mass resolution of this simulation. The present-day subhalo mass is the mass enclosed within a truncation radius, which is defined as the radius where the spherically-averaged density profile starts to flatten or to increase with radius. The fitting formula for the mean cumulative number of subhalos with present-day (observed) mass m_{sub} given a host halo mass M_{h} is:

$$\langle N_{\text{sub}}(> m_{\text{sub}} | M_{\text{h}}) \rangle = \mu_0 \left(\frac{\mu}{\mu_1} \right)^a \exp \left[- \left(\frac{\mu}{\mu_{\text{cut}}} \right)^b \right], \quad (9)$$

where $\mu = m_{\text{sub}}/M_{\text{h}}$ and $\{\mu_0, \mu_1, \mu_{\text{cut}}, a, b\} = \{1.15^{(\log M_{\text{h}} - 12.25)}, 0.010, 0.096, -0.935, 1.29\}$. Then, the number of subhalos of mass between $m_{\text{sub}} \pm dm_{\text{sub}}/2$ residing in host halos of mass M_{h} (the SubhCMF), is simply

$$\Phi_{\text{sub}}(m_{\text{sub}} | M_{\text{h}}) dm_{\text{sub}} = d\langle N_{\text{sub}}(> m_{\text{sub}} | M_{\text{h}}) \rangle. \quad (10)$$

The average cumulative number of subhalos reported in Boylan-Kolchin et al. (2010), Eq. (9), was actually obtained for MW-sized halos. However, as the authors discuss, the normalization factor, μ_0 , has been found to vary with M_{h} , roughly 15% per dex in M_{h} . For this reason we introduce the quantity $\mu_0 = 1.15^{(\log M_{\text{h}} - 12.25)}$ (see also Gao et al. 2011).

The difference in cosmology between the Millennium-II simulation and ours leads to differences in the resulting abundances of subhalos of roughly a few per cent in the amplitude of the subhalo mass function (Boylan-Kolchin et al. 2010), and it has little effects on our results (see RDA12). In any case, we introduce a correction to first order, taking advantage of the fact that Tinker et al. (2008b) provides the distinct HMF as a function of the relevant cosmological parameters. First, the subhalo mass function is calculated from Eqs. (9) and (10) and the Tinker et al. (2008b) HMF defined for the Millenium cosmology. Then, the "Millenium-cosmology" subhalo-to-halo mass function ratio is calculated, $T(M) = \phi_{\text{sub, MII}}(M)/\phi_{\text{h, MII}}(M)$. This ratio is now used to recalculate the subhalo mass function for our cosmology as $\phi_{\text{sub}}(M) = T(M)\phi_{\text{h}}(M)$, where $\phi_{\text{h}}(M)$ is the Tinker et al. (2008b) HMF for our cosmology. Finally, assuming the same functional form for the subhalo conditional mass function (Eq. 10), with the same μ_0 , we obtain the new parameters for our cosmology from χ^2 fitting $\{\mu_1, \mu_{\text{cut}}, a, b\} = \{0.011, 0.096, -0.935, 1.342\}$. These are actually very close to what is reported in Boylan-Kolchin et al. (2010).

Analogously to centrals, for constructing the satellite GSMF we introduce the probability, $P_{\text{sat}}(M_* | m_{\text{sub}}) dM_*$, that a subhalo of mass m_{sub} hosts a satellite galaxy with stellar mass between $M_* \pm dM_*/2$. In general there is no reason for assuming $P_{\text{cen}}(M_* | M_{\text{h}}) = P_{\text{sat}}(M_* | m_{\text{sub}})$ ¹.

¹ This assumption may actually lead to inconsistent results, even

We again adopt a log-normal form,

$$P_{\text{sat}}(M_* | m_{\text{sub}}) dM_* = \frac{dM_*}{\sqrt{2\pi\sigma_s^2} M_* \ln(10)} \times \exp \left[- \frac{\log^2(M_*/M_{*,s}(m_{\text{sub}}))}{2\sigma_s^2} \right], \quad (11)$$

where σ_s is the scatter (width) around the logarithm in base 10 of $M_{*,s}(m_{\text{sub}})$, the mean satellite-subhalo mass relation (SSMR). Similarly to centrals, we parametrize $\log M_{*,s}(m_{\text{sub}})$ using Eq. (5). The reason is because, as observations suggest, the shape of the satellite GSMF is also a Schechter-like function (e.g., YMB09; Yang et al. 2012), which is easily reproduced from the halo or subhalo mass function using the parametrization given by Eq. (5).

The next step is to link satellites to subhalos. The most natural way to do this is via their occupational numbers (e.g., Yang, Mo & van den Bosch 2009b). Let $\Phi_{\text{sat}}(M_* | M_{\text{h}})$ be the CSMF giving the mean number of satellites of stellar mass $M_* \pm M_*/2$ residing in a host halo of mass M_{h} :

$$\Phi_{\text{sat}}(M_* | M_{\text{h}}) dM_* = dM_* \int_0^{\infty} P_{\text{sat}}(M_* | m_{\text{sub}}) \Phi_{\text{sub}}(m_{\text{sub}} | M_{\text{h}}) dm_{\text{sub}}. \quad (12)$$

The similarity with Eq. (7) is not a coincidence, since this is actually the AMT in its differential form but at the level of CSMFs. Integrating this over stellar mass gives the mean occupation of satellite galaxies in individual halos:

$$\langle N_s(> M_* | M_{\text{h}}) \rangle = \int_{M_*}^{\infty} \Phi_{\text{sat}}(M_* | M_{\text{h}}) dM_*. \quad (13)$$

At this point we are in a position to compute the satellite GSMF:

$$\phi_{g,\text{sat}}(M_*) dM_* = dM_* \int_0^{\infty} \Phi_{\text{sat}}(M_* | M_{\text{h}}) \phi_{\text{h}}(M_{\text{h}}) dM_{\text{h}}, \quad (14)$$

and in the case that σ_s is a constant,

$$\phi_{g,\text{sat}}(M_*) dM_* = dM_* \int_0^{\infty} P_{\text{sat}}(M_* | m_{\text{sub}}) \phi_{\text{sub}}(m_{\text{sub}}) dm_{\text{sub}}, \quad (15)$$

which is the matching of satellite galaxies to subhalos. The mean number density of satellite galaxies with stellar mass greater than M_* is given by:

$$n_{g,\text{sat}}(> M_*) = \int_0^{\infty} \langle N_s(> M_* | M_{\text{h}}) \rangle \phi_{\text{h}}(M_{\text{h}}) dM_{\text{h}}. \quad (16)$$

for the accretion-time m_{sub} definition, as shown in RDA12. For m_{sub} defined at the present time, tidal stripping affects the masses of the subhalos producing this obviously a systematic offset between the galaxy-halo and satellite-subhalo mass relations, which is sometimes incorporated as an assumed global offset in the AMT analyses (e.g., Vale & Ostriker 2004; Weinberg et al. 2008). For m_{sub} defined at the accretion epoch, the two relations become actually close according to the extended AMT analysis of RDA12 or to the results of cosmological simulations (Simha et al. 2012), but there may be still offsets and differences in scatter because of the uncertain evolution of the satellites after accretion (see Fig. 2 in RDA12 and Figs. 3 and 7 below).

Finally, note that the relation between $P_{\text{cen}}(M_*|M_{\text{h}})$ and $P_{\text{sat}}(M_*|m_{\text{sub}})$ with the distribution $P(M_*|M)$ used in the standard AMT (e.g., Vale & Ostriker 2008; Behroozi, Conroy & Wechsler 2010) is given by

$$P(M_*|M) = \frac{\phi_{\text{sub}}(M)}{\phi_{\text{DM}}(M)} P_{\text{sat}}(M_*|M) + \frac{\phi_{\text{h}}(M)}{\phi_{\text{DM}}(M)} P_{\text{cen}}(M_*|M), \quad (17)$$

where $\phi_{\text{DM}}(M) = \phi_{\text{sub}}(M) + \phi_{\text{h}}(M)$ and M applies either to the distinct halo or subhalo masses. Then, the above equation relates the mass relation commonly obtained through the standard AMT with those obtained in this paper,

$$\langle \log M_*(M) \rangle = \frac{\phi_{\text{sub}}(M)}{\phi_{\text{DM}}(M)} \langle \log M_{*,\text{s}}(M) \rangle + \frac{\phi_{\text{h}}(M)}{\phi_{\text{DM}}(M)} \langle \log M_{*,\text{c}}(M) \rangle, \quad (18)$$

where $M_{*,\text{s}}(M)$ and $M_{*,\text{c}}(M)$ are the SSMR and CHMR, respectively. It is worth noting that the standard AMT is recovered if both $P_{\text{cen}}(M_*|M_{\text{h}})$ and $P_{\text{sat}}(M_*|m_{\text{sub}})$ are assumed to be δ -functions. Then $n_{g,\text{cen}}(> M_*) + n_{g,\text{sat}}(> M_*) = n_{\text{sub}}(> M_{\text{h}}) + n_{\text{h}}(> M_{\text{h}})$. For a detailed discussion see RDA12.

2.2. The two-point correlation function

So far, the galaxy-(sub)halo link is based on an extended AMT. However, having modeled the occupational numbers for central and satellite galaxies, we can now introduce information related to the spatial clustering. For convenience, we will write $\langle N \rangle \equiv \langle N(> M_*|M_{\text{h}}) \rangle$, $\langle N_{\text{c}} \rangle \equiv \langle N_{\text{c}}(> M_*|M_{\text{h}}) \rangle$ and $\langle N_{\text{s}} \rangle \equiv \langle N_{\text{s}}(> M_*|M_{\text{h}}) \rangle$.

As usual, the two-point correlation function is decomposed into two parts,

$$1 + \xi_{\text{gg}}(r) = [1 + \xi_{\text{gg}}^{\text{1h}}(r)] + [1 + \xi_{\text{gg}}^{\text{2h}}(r)], \quad (19)$$

where $\xi_{\text{gg}}^{\text{1h}}(r)$ describes pairs within the same halo (one-halo term), while $\xi_{\text{gg}}^{\text{2h}}(r)$ describes pairs occupying different haloes (two-halo term).

To compute the one-halo term, we need to count all galaxy pairs $\langle N(N-1) \rangle / 2$ separated by a distance $r \pm dr/2$ within individual halos of mass M_{h} , following a pair distribution $\lambda(r)dr$ weighted by the abundance of distinct halos, ϕ_{h} , and normalized by the mean galaxy number density n_g ,

$$1 + \xi_{\text{gg}}^{\text{1h}}(r) = \frac{1}{2\pi r^2 n_g^2} \int_0^\infty \frac{\langle N(N-1) \rangle}{2} \lambda(r) \phi_{\text{h}}(M_{\text{h}}) dM_{\text{h}} \quad (20)$$

The contribution to the mean number of galaxy pairs from central-satellite pairs and satellite-satellite pairs is given by

$$\begin{aligned} \frac{\langle N(N-1) \rangle}{2} \lambda(r) dr &= \langle N_{\text{c}} \rangle \langle N_{\text{s}} \rangle \lambda_{\text{c},\text{s}}(r) dr \\ &+ \frac{\langle N_{\text{s}}(N_{\text{s}}-1) \rangle}{2} \lambda_{\text{s},\text{s}}(r) dr. \end{aligned} \quad (21)$$

We assume that central-satellite pairs follow a pair distribution function $\lambda_{\text{c},\text{s}}(r)dr = 4\pi\tilde{\rho}_{\text{NFW}}(M_{\text{h}},r)r^2dr$, where $\tilde{\rho}_{\text{NFW}}(M_{\text{h}},r)$ is the normalized NFW halo density profile. The satellite-satellite pair distribution, $\lambda_{\text{s},\text{s}}(r)dr$, is

then the normalized density profile convolved with itself, that is, $\lambda_{\text{s},\text{s}}(r)dr = 4\pi\lambda_{\text{NFW}}(M_{\text{h}},r)r^2dr$, where λ_{NFW} is the NFW profile convolved with itself. An analytic expression for $\lambda_{\text{NFW}}(M_{\text{h}},r)$ is given by Sheth et al. (2001). Both $\tilde{\rho}_{\text{NFW}}$ and λ_{NFW} depend on the halo concentration parameter, c_{NFW} . N-body numerical simulations show that this parameter weakly anti-correlates with mass, $c_{\text{NFW}} = a - b \times \log M_{\text{h}}$, though with a large scatter.

Based on results of N -body (Kravtsov et al. 2004) and hydrodynamic (Zheng et al. 2005) simulations, we will assume that the number of satellite-satellite pairs follow a Poisson distribution with mean $\langle N_{\text{s}} \rangle^2 = \langle N_{\text{s}}(N_{\text{s}}-1) \rangle$. This is also supported by the analysis based on a large catalog of galaxy groups by Yang, Mo & van den Bosch (2008).

For the two-halo term, where $r > 2R_{\text{h}}(M_{\text{h}})$, all pairs must come from galaxies in separate halos. We compute the two-halo term from the non-linear matter correlation function, $\xi_m(r)$ following (Smith et al. 2003):

$$\xi_{\text{gg}}^{\text{2h}}(r) = b_g^2 \zeta^2(r) \xi_m(r), \quad (22)$$

where $\zeta(r)$ is the scale dependence of dark matter halo bias (Tinker et al. 2005, see their Eq. B7), and,

$$b_g = \frac{1}{n_g} \int_0^\infty b(M_{\text{h}}) \langle N(> M_*|M_{\text{h}}) \rangle \phi_{\text{h}}(M_{\text{h}}) dM_{\text{h}}, \quad (23)$$

is the galaxy bias with $b(M_{\text{h}})$ being the halo bias function (Sheth, Mo & Tormen 2001).

Once we have calculated $\xi_{\text{gg}}(r)$, we relate it to the projected two-point correlation function (2PCF), $w_{\text{p}}(r_{\text{p}})$, by

$$w_{\text{p}}(r_{\text{p}}) = 2 \int_0^\infty \xi_{\text{gg}}(\sqrt{r_{\text{p}}^2 + x^2}) dx. \quad (24)$$

In this model, Eqs. (20–24) relate the observed 2PCF to the central and satellite occupational number distributions, which on their own are related to the central and satellite-(sub)halo mass relations. In consequence, the correlation function is related to the total GSMF and its decomposition into centrals and satellites. Therefore, since the GSMFs and PCFs are tightly connected, any combination of these observational constraints is not expected to provide independent constraints on the mass relations and the occupational number distributions. However, we expect that the uncertainties in the determinations of these functions are reduced as more observational constraints are introduced. We will explore this question in more detail in §§4.1.

2.3. Parameters in the model

Ultimately, our model, which in total consists of ten free parameters –if σ_{c} , σ_{s} , and the $c_{\text{NFW}} - M_{\text{h}}$ relation are fixed– constrains the central and satellite stellar-to-(sub)halo mass relations. Five parameters are to model the CHMR (Eq. 5): $M_{1,\text{c}}$, ϵ_{c} , α_{c} , δ_{c} , and γ_{c} ; and five more to model the SSMR (and therefore the satellite occupational numbers): $m_{1,\text{s}}$, ϵ_{s} , α_{s} , δ_{s} , and γ_{s} . Note that the success of our model relies on the ability to choose a parametric description of the $M_* - M_{\text{h}}$ and $M_* - m_{\text{sub}}$ relations (Eq. 5), such that the observed total GSMF and its decomposition into centrals and satellites are well-reproduced. As discussed previously, the main motiva-

TABLE 1
CONSTRAINTS

Constraints:						
Data set	Satellite GSMF	Central GSMF	Total GSMF	2PCF	χ^2	
A	YMB09	YMB09	—	\times	$\chi^2(\phi_{\text{sat}}^{\text{YMB09}}) + \chi^2(\phi_{\text{cen}}^{\text{YMB09}})$	
B	\times	\times	YMB09	Y11	$\chi^2(\phi_{\text{all}}^{\text{YMB09}}) + \chi^2(w_{\text{p,bin}}^{\text{Y11}})$	
C	YMB09	YMB09	—	Y11	$\chi^2(\phi_{\text{sat}}^{\text{YMB09}}) + \chi^2(\phi_{\text{cen}}^{\text{YMB09}}) + \chi^2(w_{\text{p,bin}}^{\text{Y11}})$	
B1	\times	\times	BGD08	Y11	$\chi^2(\phi_{\text{all}}^{\text{BGD08}}) + \chi^2(w_{\text{p,bin}}^{\text{Y11}})$	
Predictions:						
Data set	Satellite GSMF	Central GSMF	Total GSMF	2PCF	sat. CSMF	CHMR & SSMR
A	\times	\times	—	\checkmark	\checkmark	\checkmark
B	\checkmark	\checkmark	\times	\times	\checkmark	\checkmark
C	\times	\times	\times	\times	\checkmark	\checkmark
B1	\checkmark	\checkmark	\times	\times	\checkmark	\checkmark

tion for the functional forms chosen here is that they are able to reproduce Schechter-like GSMFs accurately.

Using a SDSS halo-based group catalog, YMB09 found that the intrinsic scatter around the CHMR is approximately independent of halo mass and log-normally distributed, with a mean width of $\sigma_c(\log M_h) = 0.173$ dex. This result is also supported by studies of satellite-galaxy kinematics (More et al. 2009, 2011) and analysis using HOD models (Yang, Mo & van den Bosch 2003; Cooray 2006; Cacciato et al. 2009; Leauthaud et al. 2012). Additionally, AMT results are able to reproduce the GSMF and the spatial clustering of galaxies simultaneously when using $\sigma_c = \text{const.}$ (e.g., Moster et al. 2010; RDA12; Reddick et al. 2012). On the other hand, the scatter σ_s around the SSMR has not yet been discussed in the literature. In RDA12 it is assumed to be the same as for central galaxies, giving results consistent with the observed projected 2PCFs and satellite CSMFs. Having said that, we assume the intrinsic scatters σ_c and σ_s to be independent of halo mass and equal to 0.173 dex. Nevertheless, as we have discussed, the constraints provided by the GSMF decomposed into centrals and satellites and the projected 2PCFs are not independent but rather they are complementary. Therefore, when using all these constraints, it may be possible to leave σ_c and/or σ_s as free parameters. We will perform this exercise in Section 3.3. Finally, for the relation of the concentration parameter c_{NFW} with mass, we use the fit to numerical simulations by Muñoz-Cuartas et al. (2011).

2.4. Observational data sets and strategy

A combination of the total, central, and satellite GSMFs, and the projected 2PCF for different M_* bins are necessary to constrain our model. In the following, we will experiment with different combinations of these data. We wish to understand how the stellar-(sub)halo mass relations vary depending on the combination of observational data used to constrain them. In particular, we would like to explore whether the uncertainty in the model parameters drops significantly by introducing more observational constraints.

The different observational data to be used for constraining the model parameters are as follows:

- The YMB09 GSMF decomposed into central and satellite galaxies. These data were obtained from a

large halo-based galaxy group catalog constructed in Yang et al. (2007) from the SDSS DR4 (they define a central galaxy as the most massive galaxy in a group with the remaining galaxies being satellites). Both the central and the satellite GSMF are well-described by Schechter functions, with central galaxies being the more abundant population at all masses, at least above the low-mass limit of the sample, $\log(M_*/M_\odot) = 8.4$.

- The total BGD08 GSMF, which is well described by a double Schechter function. This GSMF is steeper at the low-mass end than the YMB09 GSMF (See also Drory et al. 2009). BGD08 have actually extended the GSMF to a lower limit, $\log(M_*/M_\odot) = 7.4$, by introducing a surface-brightness completeness correction.
- The projected 2PCFs determined in five M_* bins by Yang et al. (2012, hereafter Y12) based on the SDSS DR7.

The combinations explored to constrain the model parameters consists of four data sets:

Set A consists of the YMB09 central and satellite GSMFs, and is used to constrain the model parameters of our extended AMT; in this case, the projected 2PCFs in various mass bins are predicted. Set B consists of the *total* YMB09 GSMF and the Y12 projected 2PCFs, and this is used to constrain our full combined model; the GSMF decomposed into centrals and satellites is a prediction. Set B1 is similar to set B but instead of the YMB09 GSMF, the Baldry, Glazebrook & Driver (2008, hereafter BGD08) GSMF is used. Set C consists of all the available data: the YMB09 GSMF *decomposed into centrals/satellites* and the Y12 projected 2PCF determined in different M_* bins; this data set over-constrains our full combined model.

We notice that fiber collisions in the SDSS data underlying the group catalog may introduce an extra source of uncertainty when using the satellite GSMF for constraining the parameters in sets A and C. However, this seems to be a small effect at most since YMB09 show that satellite CSMFs with a correction for fiber collisions are only marginally different. It is also important to highlight that the authors report only the diagonal elements of the covariance matrix for the projected 2PCFs. We expect

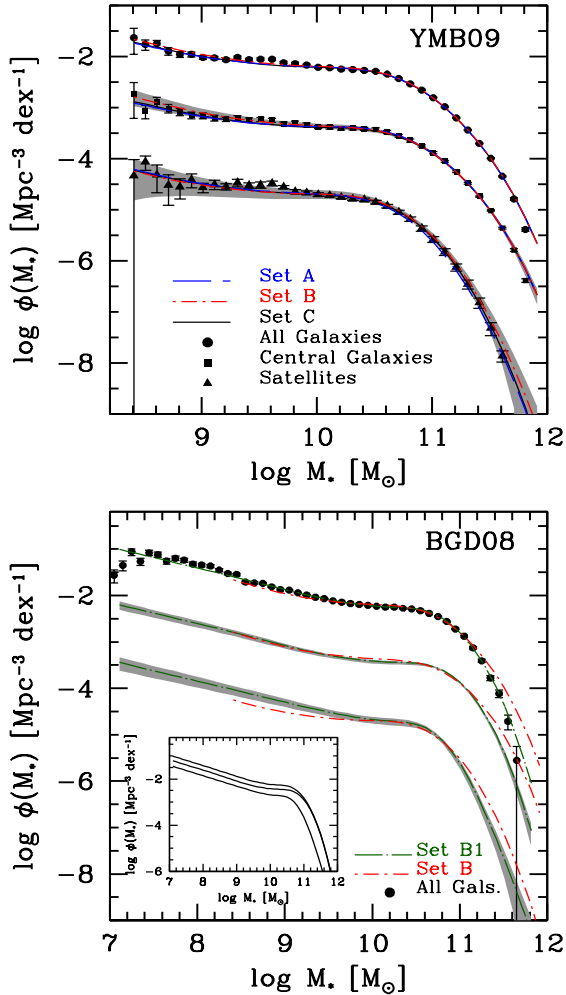


FIG. 1.— The GSMF for all, central, and satellite galaxies. For clarity, in each panel the central GSMF was shifted down by 1 dex, and the satellite GSMF by 2 dex. *Upper panel:* Model results for sets A (blue long dashed line), B (red dot-short-dashed line), and C (solid line), compared to the observed YMB09 GSMFs for all (filled circles), central (filled squares), and satellite galaxies (filled triangles). For sets A and C the curves are just the best joint fit to the data, while for set B are model predictions. The shaded areas correspond to the standard deviation of the 1.5×10^6 MCMC models for set B. *Lower panel:* Same as upper panel but for the set B1 (green dot-long-dashed line and shaded areas). The predictions for set B are repeated in this panel (red dot-short-dashed line). The corresponding observational total BGD08 GSMF is shown with solid circles and error bars. The inset shows how the central and the satellite GSMFs add up to give the total GSMF in the case of set B1.

that the the full covariance matrix would reduce possible systematic errors and extra uncertainties in some of the constrained parameters. As discussed in §3.1, the lack of the covariance matrix seems to affect the results for the abundance of satellite galaxies, however, these effects are of minor importance.

Table 1 summarizes the different data sets presented above and specifies where the observables are used as constraints and in where they are predicted by the model.

We use Markov Chain Monte Carlo (MCMC) methods for sampling the best fit parameters that maximize the likelihood function $\mathcal{L} \propto \exp(-\chi^2/2)$. Each MCMC chain consist of 1.5×10^6 elements. See Appendix A for details on the full procedure.

3. THE ANALYSIS

In our model the central/satellite GSMFs are tightly connected to the projected 2PCFs in such a way that given the former the latter can be inferred and vice versa (§§3.1). This connection passes through the underlying halo/subhalo statistics and the stellar-to-(sub)halo mass relations. Therefore, the latter, together with the satellite CSMF, are predictions in all cases (§§3.2 and §4, respectively).

3.1. The GSMFs & projected 2PCFs

Figure 1 shows the model results for the central, satellite, and total GSMFs, while Fig. 2 shows the projected 2PCFs in different mass bins. The observational data are also plotted in these figures (symbols with error bars). The shaded regions in the figures are the resulting model-fit standard deviations calculated from the 1.5×10^6 MCMC models for sets B and B1 (the upper and lower panels of Fig. 1, respectively), and for set A (Fig. 2). These standard deviations are associated with the uncertainties in the model parameters, and are produced partially by the uncertainties in the observations used to constrain the model. For a discussion on the model scatter see Sect. 5.1.

For set A, which is constrained by the YMB09 satellite and central GSMFs (solid symbols in Fig. 1; red dot-dashed curves are just the joint best fits to data), the model predicts the projected 2PCFs (red dot-dashed curves with shaded areas in Fig. 2). Both the amplitude and the shape of the predicted projected 2PCFs are in excellent agreement with observations (crosses with error bars, Y12) at each stellar mass bin plotted in Fig. 2. This result is not surprising as shown in RDA12. What is interesting, however, is that the standard deviations are consistent with the errors reported in the observations. Note that the 1-halo term is the zone with the largest uncertainty, which arises directly from the uncertainty in the satellite GSMF. For set B, which is constrained by the total YMB09 GSMF and the Y12 projected 2PCFs (black curves are just the joint best fits to data), the model predicts the central and satellite GSMFs (black curves and gray shaded regions in the upper panel of Fig. 1). The model predictions agree very well with observations, and therefore with set A. These results show that *the central/satellite GSMFs and the 2PCFs are tightly connected in such a way that given one, the other can be inferred through our model*. Observe that in Fig. 1, the standard deviations are consistent with the error bars both for the satellite and the central GSMF. The former has the largest uncertainties. Therefore, the lack of information from the projected 2PCF covariance matrix seems to affect mostly the abundance of satellite galaxies or equivalently, the 1-halo term in the projected 2PCF.

Set B1 (lower panel of Fig. 1) is similar to set B, but the BGD08 total GSMF is used as a constraint instead of YMB09 data. Therefore, the model total GSMF and 2PCFs (green dot-long-dashed curves in Figs. 1 and 2, respectively) are just the joint best fits to the data, but the central and satellite GSMFs are predicted (green dot-long-dashed curves with gray shaded areas in the lower panel of Fig. 1). Note that the BGD08 GSMF extends to lower stellar masses. The resulting slope of the

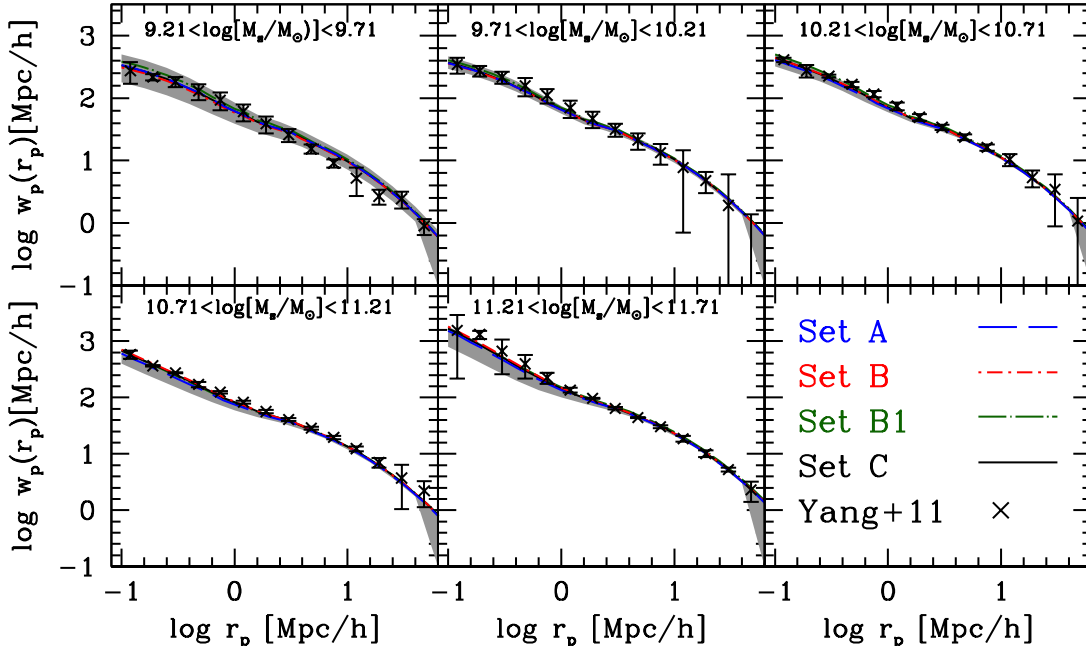


FIG. 2.— Projected 2PCFs in five stellar mass bins corresponding to the data sets A, B, C, and B1 (see Table 1), and to the Y12 observational determinations (crosses with error bars). The lines corresponding to each set are indicated in the last panel. For set A, the plotted 2PCFs are predictions, while for the rest of the sets are just the joint best fits. The shaded area show the standard deviation for the 1.5×10^6 MCMC models.

satellite GSMF at the faint end ($\log(M_*/M_\odot) \lesssim 9.6$), is $\alpha \sim -1.5$, which is steeper than set B, $\alpha \sim -1.2$, and the bump around $M^* \sim 8 \times 10^{10} M_\odot$ in the central GSMF is more pronounced. A steeper total GSMF implies a major contribution of satellite galaxies to the total GSMF at low masses.

Finally, for set C, neither the central/satellite GSMFs nor the projected 2PCFs at different mass bins are predicted but rather employed to constrain the model parameters. Therefore, the blue long-dashed curves shown for set C in Figs. 1 and 2 are just the joint best fits to the observations; they are not predictions. For this set, the predictions are the constraints on the stellar-to-(sub)halo mass relations. The question now is how different can these relations and their uncertainties be from those inferred using the other data sets.

3.2. Mass relations

In the upper panels of Fig. 3 we plot the central, satellite, and average stellar-to-(sub)halo mass ratios (stellar mass fractions, f_*) as a function of the (sub)halo mass obtained for each data set listed in Table 1. The stellar mass fractions are obtained directly from the corresponding mass relations. Table 2 lists the best fit MCMC model parameters of these relations for each of the sets. We use Eq. (18) to compute the average f_* . Recall that the average relation, $\langle \log M_*(M) \rangle$, is conceptually what is commonly obtained with the standard AMT. However, in the latter case it is not possible to distinguish the mass relations for centrals and satellites, and it is common practice to assume them equal. As shown in RDA12, this assumption is not correct.

In general, we find that the shape of the stellar fractions for both the centrals/halos and satellites/subhalos rises steeply at low masses, reaching a maximum and

then declines roughly as a power law towards higher masses. We do not find significant differences among the stellar mass fractions obtained for sets A, B and C. Observe how all of them lie well within the 1σ uncertainty which is dominated by the systematic uncertainty in the stellar mass determination (~ 0.25 dex, light shaded area in Fig. 3; see Behroozi, Conroy & Wechsler 2010). All these relations even lie well within the standard deviation of the MCMC models, shown as a dark gray shaded area in set C (the others being very similar). In the lower panels of Fig. 3 we plot the the standard deviations as a function of (sub)halo mass for each set, which we discuss in detail in §5.1.

We arrive at two important implications: (1) the very small standard deviations obtained for the stellar-to-(sub)halo mass relations implies that the assumption that on average there is a monotonic relation between galaxy and (sub)halo masses is consistent with the data; (2) the result that set A and set B lead to very similar mass relations confirms that *matching abundances is equivalent to matching occupational numbers and vice versa*, as suggested in RDA12. Therefore, constraining the model parameters with all the observational information, as in set C, should lead again to the same stellar-to-(sub)halo mass relations as in sets A and B. Indeed, this is what we obtain.

The central f_*-M_h relations for sets A–C at the low (high) mass end scale roughly as $f_* \propto M_h^{1.5}$ ($f_* \propto M_h^{-0.7}$). The average f_*-M_h relations are such that they lie above but closer to centrals, simply because they are the dominant population. Instead, the satellite f_*-m_{sub} relations are quite different to centrals, both in the amplitude and in the location of the maximum of f_* . The maximum shifts from $\log(M_h/M_\odot) \approx 11.9$ to

TABLE 2
FIT PARAMETERS

Central galaxies:										
Data set	$\log M_{1,c}$	stdev	$\log \epsilon_c$	stdev	α_c	stdev	δ_c	stdev	γ_c	stdev
A	11.477	0.073	-1.582	0.050	2.252	0.461	3.558	0.206	0.485	0.044
B	11.480	0.066	-1.580	0.038	1.982	0.338	3.530	0.198	0.491	0.040
C	11.493	0.068	-1.600	0.047	2.138	0.417	3.572	0.202	0.487	0.043
B1	11.676	0.056	-1.475	0.027	2.056	0.110	2.454	0.183	0.514	0.047
Satellite galaxies:										
Data set	$\log m_{1,s}$	stdev	$\log \epsilon_s$	stdev	α_s	stdev	δ_s	stdev	γ_s	stdev
A	10.761	0.069	-0.992	0.063	2.469	0.710	3.616	0.260	0.435	0.077
B	10.773	0.088	-0.951	0.052	2.670	0.792	3.612	0.255	0.437	0.075
C	10.775	0.064	-0.957	0.052	2.474	0.657	3.586	0.260	0.423	0.071
B1	11.017	0.90	-0.709	0.044	2.322	0.191	1.667	0.225	0.993	0.133

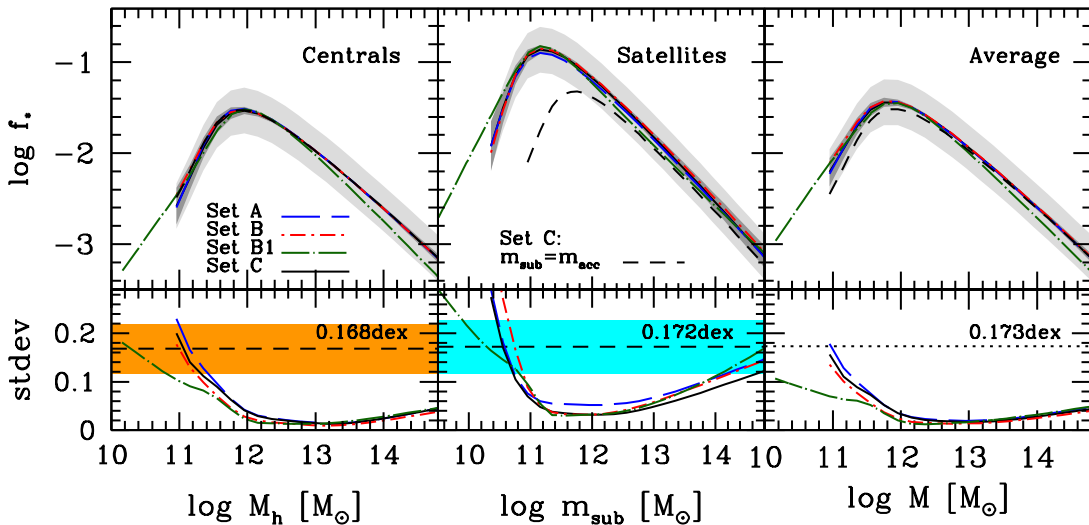


FIG. 3.— *Upper panels:* From left to right, the constrained stellar mass fractions of central and satellites, and of the number-density average (Eq. 18) of both. The lines corresponding to each set are indicated inside the panels. Short-dashed curves in the second and third panels are the constrained mass relations when the subhalo mass is defined at its accretion time. The systematic uncertainty due to the uncertainty in the stellar mass determination (0.25 dex) is shown with the light-gray shaded areas. Gray dashed areas indicate the MCMC model-fit standard deviation in the case of set C. *Lower panels:* The MCMC model-fit standard deviations for each data set. The short dashed lines in the right and middle lower panels are the intrinsic scatters, σ_c and σ_s , constrained for the set C assuming them to be constant. The color shaded area show the standard deviations of these values.

$\log(m_{\text{sub}}/M_{\odot}) \approx 11.2$. These differences are basically due to the fact that subhalos lose mass due to tidal stripping (on average 60–65% of the mass since the accretion for subhalos hosting satellites less massive than $\sim 2 \times 10^{11} M_{\odot}$; RDA12; see also Vale & Ostriker 2004; Weinberg et al. 2008; Watson, Berlind & Zentner 2012). However, even when the subhalo mass at accretion time is used, some differences remain, showing that the assumptions about evolution made in order to construct the nominal SSMR for this case are roughly but not exactly obeyed.

In Fig. 3 we plot the model results for subhalo mass defined at accretion time for the set C (black dashed curve)². The f_*-m_{sub} (or SSMR) relation now lies close to the central f_*-M_h (or CHMR) relation. Recall that

² The SubhCMF for subhalos defined at the accretion time given by Boylan-Kolchin et al. (2010, see also Giocoli, Tormen & van den Bosch 2008) has been used (see RDA12 for details).

for connecting the present-day observed satellite M_* to (sub)halo masses at their different accretion epochs, one implicitly assumes that the satellite stellar masses change in a way that at $z = 0$ the SSMR is equal to the CHMR. Our ignorance about how the satellite masses evolve introduces an extra uncertainty in the determination of the SSMR when the subhalo mass at the accretion time is used (Y12; RDA12). In any case, as extensively discussed in RDA12, for one or another definition of subhalo mass, there is a unique but different average SSMR for which the satellite GSMF and CSMF, and the correlation functions are in agreement with observations. Nevertheless, when the SSMR is assumed to be equal to the CHMR, the predicted satellite GSMF and CSMF, and correlation functions depart from observations. They do so more strongly for the observation-time definition, m_{obs} , and less strongly for the accretion-time definition, m_{acc} (see Figs. 1, 3, and 4 in RDA12).

The mass relations for set B1 (green dot-dashed curves) are somewhat different to those of set B: at high masses

the central (and the average) f_*-M_h relation is steeper than in set B, and at low masses the satellite f_*-m_{sub} relation is shallower. Recall that the massive-end of the total BGD08 GSMF (set B1) decays faster than in the YMB09 GSMF (set B; see Fig. 1). Consequently, at a fixed M_h the CHMR for set B1 is systematically lower than for set B. At low masses, the GSMF in set B1 is steeper than in set B, causing this a steeper satellite GSMF and therefore a shallower decay of M_* as m_{sub} decreases as compared to set B.

3.3. Constraining the intrinsic scatter of the stellar-to-(sub)halo mass relations

The results presented above are obtained under the assumption of lognormal intrinsic scatter around the CHMR and the SSMR with constant 1σ widths of 0.173 dex for both relations. Our model is over-constrained by observations in set C. Therefore, we may leave one or both of the intrinsic scatters as free parameters, but keep the assumption that they are constant, that is, independent of (sub)halo mass.

The results of leaving only one of σ_c or σ_s free are very similar to leaving both free at the same time. The MCMC algorithm in the latter case constrains the intrinsic scatters to be $\sigma_c = 0.168 \pm 0.051$ dex and $\sigma_s = 0.172 \pm 0.057$ dex. These values are surprisingly close to those we have assumed. These values are plotted in the lower panels of Fig. 3. The constrained mass relation parameters also remain almost the same. So, under the assumption of lognormal distributed and constant intrinsic scatters, our results confirm previously estimated values of the scatter for central galaxies, and predict similar values for the scatter around the mass relation of satellite galaxies.

4. OCCUPATIONAL STATISTICS

The mass relations we obtain in the previous section allow us to explore several implications that come about naturally within the framework of our model, in particular the halo occupational statistics. In this section we study the implications for the conditional stellar mass functions, the mass distribution of the most massive satellite at a fixed halo mass, and the occurrence of Magellanic-Clouds (MC) sized galaxies in MW-sized halos.

4.1. The conditional stellar mass functions

In Fig. 4, we plot the resulting central galaxy mass probability distributions, P_{cen} , and the satellite CSMFs, Φ_{sat} , in eight halo mass bins both for set C (dark red and dark gray areas, respectively) and set B1 (orange and light gray areas, respectively). Because the predictions for sets A and B are very similar to those of set C we do not plot them separately. In fact, what is plotted in Fig. 4 are the standard deviations (scatters) of the MCMC models for each set, which for P_{cen} are actually very small. P_{cen} is the probability distribution for a halo of a fixed mass to host a central galaxy of a given stellar mass (eq. 4), while Φ_{sat} refers to the mean number of satellite galaxies residing in a host halo of a fixed mass (eq. 12). We compute P_{cen} averaged in each $[M_{h1}, M_{h2}]$

bin as:

$$\langle P_{\text{cen}} \rangle = \frac{\int_{M_{h1}}^{M_{h2}} P_{\text{cen}}(M_*|M_h)\phi_h(M_h)dM_h}{\int_{M_{h1}}^{M_{h2}} \phi_h(M_h)dM_h}, \quad (25)$$

while for satellites, the averaged CSMF is given by:

$$\langle \Phi_{\text{sat}} \rangle = \frac{\int_{M_{h1}}^{M_{h2}} \Phi_{\text{sat}}(M_*|M_h)\phi_h(M_h)dM_h}{\int_{M_{h1}}^{M_{h2}} \phi_h(M_h)dM_h}. \quad (26)$$

As seen in Fig. 4, the smaller the halo mass, the larger is the stellar mass gap between the most common central galaxy and the most abundant satellites. In other words, on average, as smaller is the halo, the larger is the ratio of the central galaxy mass to the masses of the satellite population.

In Fig. 4 we also show the corresponding observational results by YMB09 for centrals (crosses) and satellites (filled squares). The agreement between the model predictions for set C and the observational data is remarkable. However, some marginal differences are observed. As the halo mass decreases, the width of the central probability distribution is systematically somewhat broader, and therefore its amplitude is lower compared with the YMB09 data. This could be due to the assumption that the intrinsic scatter σ_c is independent of M_h . There are some pieces of evidence that σ_c slightly depends on M_h as discussed in Yang, Mo & van den Bosch (2009a, see also Zheng, Coil & Zehavi 2007).

Regarding the satellite CSMFs, the abundance of very massive satellites is slightly, but systematically, overestimated for $M_h \lesssim 10^{13}M_\odot$. This was noted already in RDA12, which suggest that a possible reason is due to the assumption that the intrinsic scatter σ_s is independent of M_h . We have explored this possibility, and found that as M_h decreases, the scatter σ_s does tend to zero in order to reproduce the observations. Such a behavior is not expected at all. Another possibility, and the most likely, is that the YMB09 satellite GSMF is underestimated (e.g., Skibba et al. 2011; RDA12), although the results from set B indicate that the obtained satellite GSMF is consistent with observations. In any case, the excess of massive satellites in low mass halos does not contribute significantly to the total mean density of galaxies.

For set B1, we observe that P_{cen} is shifted to slightly lower values of M_* as halo mass increases when comparing with observations (and set C). This is a consequence of the observed trends of the M_*-M_h relations between set B1 and C (see Fig. 3), and it is ultimately related to the fact that the high-mass end of the BGD08 GSMF decreases faster than the YMB09 GSMF. On the other hand, the satellite CSMFs for set B1 are slightly steeper at low stellar masses to those of set C. This is a consequence of the BGD08 GSMF being steeper than that of YMB09 at low masses. Note that the uncertainty in the CSMFs for set B1 dramatically increases at the lowest masses. This is because at these masses there is no information on the 2PCF, so that the total GSMF alone poorly constraints the CSMFs. Set B1 also overestimates the abundance of massive satellites in low mass halos.

4.2. Probability distributions of satellites

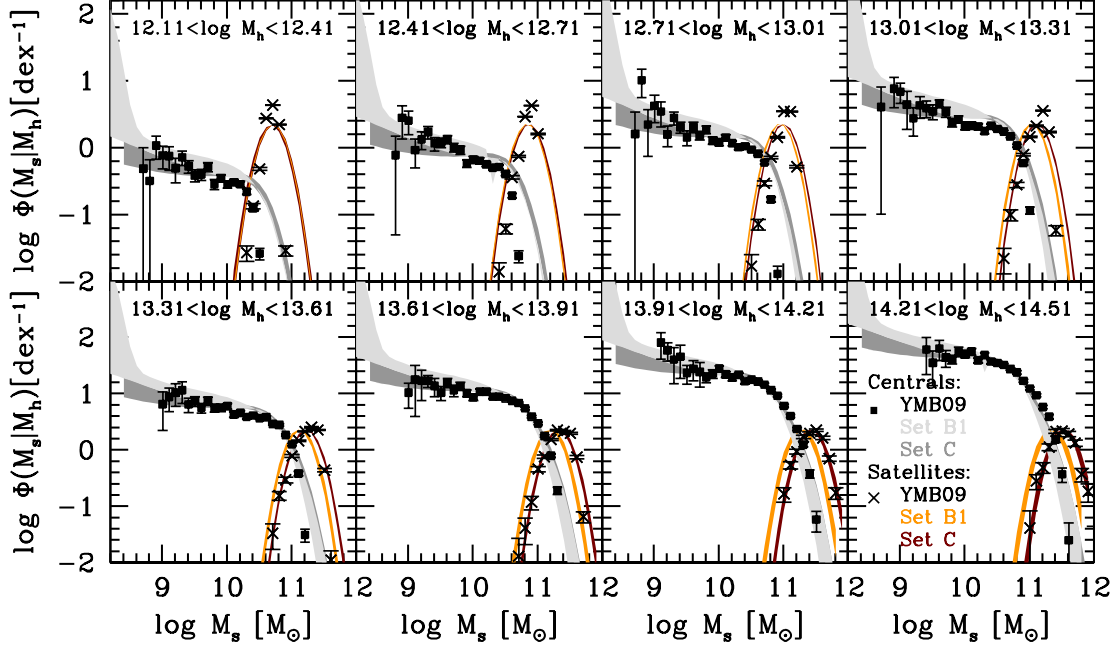


FIG. 4.— Central mass probability distributions and satellite CSMFs, P_{cen} and Φ_{sat} , in eight halo mass bins for set C (dark red and dark gray shaded areas, respectively) and set B1 (orange and light gray shaded areas, respectively). The shaded areas correspond to the standard deviation of the MCMC model-fits for each set, which for P_{cen} are actually very thin. The observational inferences by YMB09 are plotted with crosses for P_{cen} , and with filled squares for the satellite CSMFs. Their halo masses were converted to match our virial definition.

Once we have constrained the distribution of satellite galaxies, we can predict the probabilities of having N satellites of a fixed M_* or in a particular M_* range as a function of M_h . It is assumed in our model that the second moment of the satellite distribution follows a Poissonian distribution (see §§2.2); the second moment is necessary to estimate chance probabilities for any given number of satellites. The probability of finding N satellites with stellar mass above M_* in a host halo of mass M_h is then given by:

$$P(N) = \frac{N_s^N e^{-N_s}}{N!}, \quad (27)$$

where for convenience we redefined $N_s = \langle N_s(> M_* | M_h) \rangle$.

4.2.1. The most massive satellite mass distribution

We can use the satellite CSMF and Eq. (27) to compute the mass probability distribution of the most massive satellite in halos of different masses. This is given by the following expression (e.g., Milosavljević et al. 2006; Vale & Ostriker 2008):

$$\mathcal{P}_1(M_* | M_h) dM_* = \frac{\partial N_s}{\partial M_*} \times e^{-N_s} dM_*, \quad (28)$$

Note that $\int_{M_*}^{\infty} \mathcal{P}_1(M_* | M_h) dM_* = P(\geq 1)$, where $P(\geq 1)$ is the probability of finding at least one satellite galaxy more massive than M_* , $P(\geq 1) = 1 - P(0)$.

The results are shown in Fig. 5, where dashed and solid lines are for the most massive satellite and central galaxy mass distributions, respectively. The latter is by assumption a lognormal function of width $\sigma_c = 0.173$ dex. The shaded areas indicate the 68% width of the corresponding

distributions. As seen in Fig. 5, the mass distribution of the most massive satellite changes with M_h : in massive halos, it becomes closer to the distribution of the central galaxy, while in lower mass halos it tends towards small satellite masses compared to the central. This difference in masses, expressed in magnitudes, is referred in the literature of galaxy groups/clusters as the magnitude gap. The behavior seen in Fig. 5 is just a consequence of the satellite CSMFs showed in Fig. 4.

For halos larger than $\sim 1 - 3 \times 10^{13} M_{\odot}$, the mean and standard deviation of the most massive satellite mass distribution slightly increase and decrease with M_h , respectively, while for smaller masses, the mean value of $\mathcal{P}_1(M_* | M_h)$ strongly decreases as M_h decreases (faster than the central galaxy mass does) and the standard deviation increases. This transition is just at the mass corresponding to small classical galaxy groups. Therefore, our result seems to be a consequence of the fact that in groups, the larger the system’s mass is, the smaller is the collision cross sections for big galaxies of close masses so that more of them survive. Instead, in galaxy-sized halos, due to their smaller velocity dispersions, the galaxy collision cross sections are large in such a way that the largest galaxies probably merged into one dominant central. Besides, the smaller the halo, the earlier most of its mass assembled on average; hence, the (wet) mergers of the most massive galaxies in the halo would have happened early. However, a fraction of the galaxy-sized halos, while on average dynamically old, can accrete massive satellites late. This could partially explain the wide distribution of masses of the second most massive satellite in MW-sized halos. For example, as seen in Fig. 5, the probability for these halos to have the most massive satellite ~ 5 times larger than the LMC is close to the

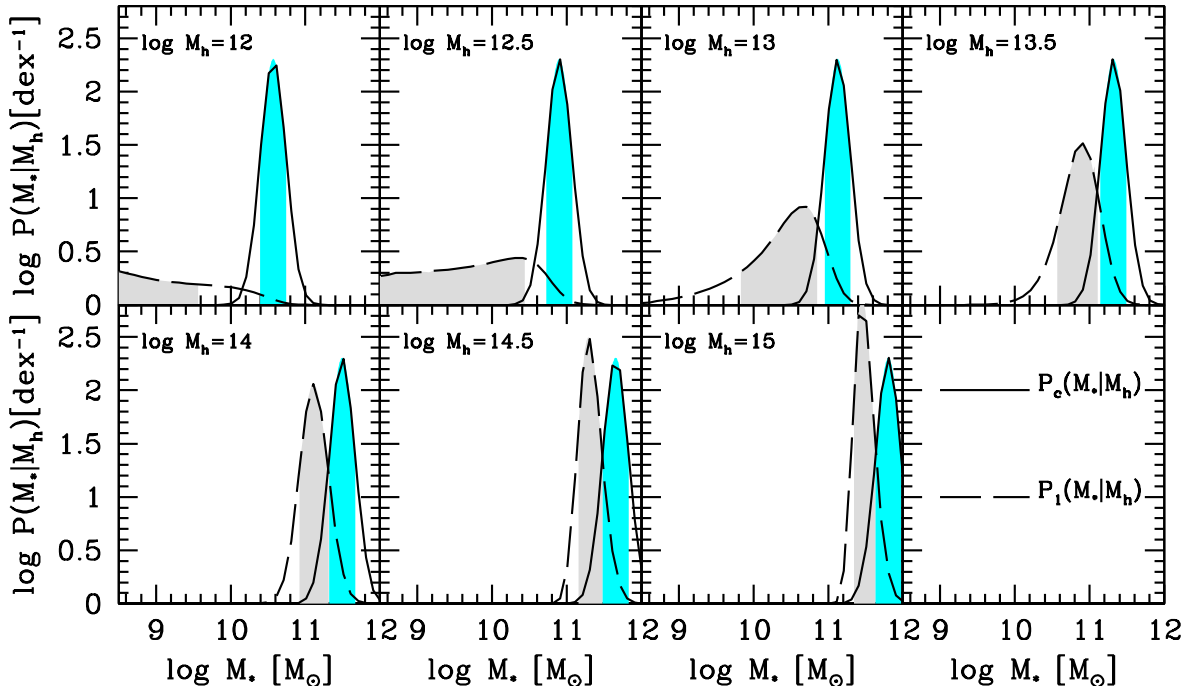


FIG. 5.— Stellar mass distributions of centrals (solid line) and the most massive satellites (dashed line) in seven different host halo masses. Shaded areas indicate the 68% of the corresponding distributions. The central galaxy masses on average are not part of the 1σ most-massive satellite distributions. For masses above $\sim 3 \times 10^{13} M_{\odot}$, only approximately 15% of both distributions overlap. For smaller masses, this fraction rapidly decreases down to 3% at $M_h = 10^{12} M_{\odot}$. The fraction of cases with overlapping distributions are expected to correspond to those cases where the central galaxy mass is a statistical realization of the most-massive satellite distribution.

probability to have this satellite as massive as the LMC.

From Fig. 4 we see that the mass of the central galaxy in the largest halos could be the statistical extreme of the satellite CSMF. The question whether the brightest cluster galaxies are a mere statistical extreme of the luminosity function in clusters or they form a different class is a longstanding one (e.g., Tremaine & Richstone 1977; Hearin et al. 2012; More 2012). According to Fig. 5, the mass distributions of the most massive satellite and central galaxy become closer as M_h increases. However, quantitatively, we see that the mean of $\mathcal{P}_1(M_*|M_h)$ lies outside of the 1σ of the central galaxy mass distribution even for a $10^{15} M_{\odot}$ halo, i.e., the central and the most massive satellite galaxy, on average, are not expected to be drawn from the same exponentially decaying mass function; this criterion is similar to the observational one introduced by Tremaine & Richstone (1977). For a similar conclusion but using a different method see Hearin et al. (2012).

We can estimate the fraction of systems where both mass distributions overlap, and consider that this fraction corresponds to the cases where the most massive satellite and the central galaxy are drawn from the same distribution. For masses above $\sim 3 \times 10^{13} M_{\odot}$, approximately 15% of halos would have central galaxies that are not statistically peculiar with respect to the satellites. For smaller masses, this fraction rapidly decreases down to 3% at $M_h = 10^{12} M_{\odot}$. In conclusion, most of centrals seem to form a statistically different class of galaxies with respect to the satellites at all halo masses, with a small fraction of cases, up to $\sim 15\%$ in cluster-sized halos, being the exception, that is to say the centrals in these

cases could be a statistical realization of the high-mass end of the satellite CSMF.

In order to compare our population statistics in detail with observations, the systems should be selected by the central galaxy M_* and/or group richness instead of the halo mass. We will carry out this exercise elsewhere by using a mock catalog based on the distributions constrained with our model.

4.2.2. The probability of Milky Way–Magellanic Clouds systems

Our model results and Eq. (28) can be used to compute the probability of having one, two, or N Magellanic Clouds (MCs) satellites in MW-sized halos. We calculate these probabilities for a range of possible MW-halo masses discussed in the literature: $(0.7, 1, 2, 3) \times 10^{12} M_{\odot}$. We use $M_{\text{LMC}} = 2.3 \times 10^9 M_{\odot}$ and $M_{\text{SMC}} = 5.3 \times 10^8 M_{\odot}$ (James & Ivory 2011) for the stellar masses of the MCs.

Firstly, we are interested in calculating statistics that can be compared with observations. From a large SDSS sample, Liu et al. (2011) have estimated the fraction of isolated galaxies with MW-like luminosities that do not have ($N_{\text{MC}} = 0$) and that have $N_{\text{MC}} = 1, 2, 3, 4, 5$, or 6 MC-sized satellites. We calculate similar probabilities for each of the halo masses mentioned above. In order to compare with Liu et al. (2011), we do not exclude systems with satellites more massive than the LMC. The results from Liu et al. (2011), for a search of MC-sized satellites up to 150 kpc around the primary, are plotted with crosses in Fig. 6 (from their Table 1)³. Note that in

³ The selection criteria and observational corrections for search-

our case satellites are counted inside the host virial radius ($\sim 200 - 300$ kpc). Liu et al. (2011) plot in their Fig. 8 the probabilities with a search radius up to 250 kpc only for $N_{\text{MC}} = 0, 1, 2, 3$. We reproduce these measurements in Fig. 6 with gray symbols and error bars.

Our predicted probabilities for set C are plotted in Fig. 6. The probabilities of MW-like halos hosting MC-sized luminous satellites (but including possible larger satellites) increases with M_h . Recall that in the case of Liu et al. (2011) the central galaxy luminosity is fixed. In this sense, our results suggest that this luminosity ($M_{0.1r} = -21.2 \pm 0.2$ mag) can be associated to halos of different masses: for those galaxies with 1 or 2 MC-sized satellites, the preferred masses are $\approx 1 - 2 \times 10^{12} M_\odot$, while for those rarer systems with 3 to 6 MC-sized satellites, the preferred masses are $> 2 \times 10^{12} M_\odot$. Interestingly enough, from the inverse of the CHMR (set C), taking into account the intrinsic scatter around this relation, the halo masses corresponding to the MW stellar mass, $\log(M_*/M_\odot) = 10.74 \pm 0.1$, are $\log(M_h/M_\odot) = 12.31 \pm 0.22$. Therefore, the rare halos that host 1 or 2 MC-sized satellites are those on the low-mass side of the halo mass distribution given the MW central stellar mass, while the much more rarer halos hosting 3 to 6 MC-sized satellites are those in the high-mass end of such a distribution.

The probability of the concrete case of two MC-sized satellites ($N_{\text{MC}}=2$; but not excluding the possibility of satellites larger than the LMC) in a MW-like halo of $2 \times 10^{12} M_\odot$ is 5.4% for set C (see Fig. 6). If we exclude now from our model predictions the possibility of having satellites larger than the LMC (as it happens in the MW system), then the probability drops to a upper limit of 2.2%.

The statistics of finding MW-sized galaxies with satellites in the concrete mass range of the MCs is limited. This statistics is actually part of the more general cumulative conditional satellite mass function. Having this function for galaxies we may then ask, for instance, whether the MW is rare because it has two too massive satellites or because it has a deficiency of massive (larger than LMC) satellites with respect to the average. We will report results related to these questions elsewhere by using a mock galaxy catalog generated with the distributions constrained here. The mock catalog will allow us also to infer several statistics given the central galaxy stellar mass in which we are interested in (e.g., the MW one) instead of exploring a range of possible halo masses as was done here.

We conclude that the agreement between the predicted and observationally determined probabilities is reasonable within the uncertainties. Such an agreement indicates that the model is self-consistent as well as consistent with the underlying Λ CDM scenario. Note that this self-consistency has been proven down to the scales of the MC galaxies and at the level of satellite population distributions. Similar probabilities were found also using large N -body cosmological simulations and looking for MW-sized halos with subhalos that have dynamical properties sim-

ing for MC-like satellites are actually quite diverse. Liu et al. (2011, see also Busha et al. 2011) explored the sensitivity of the probabilities to changes in various selection parameters and found that their results can be slightly different, being the most sensitivity to the satellite search radius around the primary.

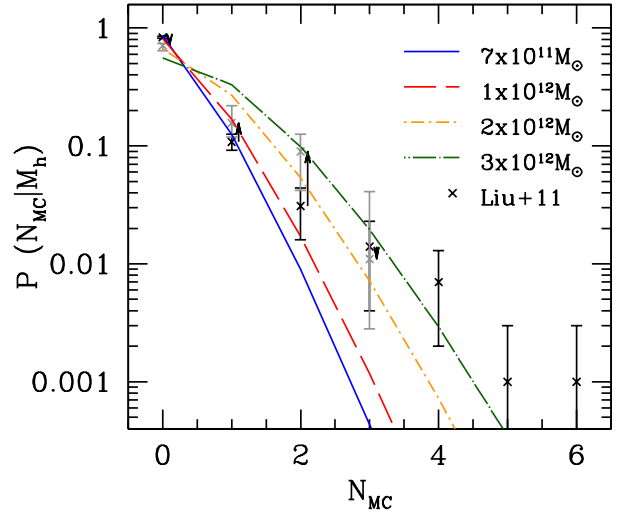


FIG. 6.— Probability of occurrence of N_{MC} MC-sized satellites in a range of possible MW-sized host halos (different lines are for the different masses indicated in the plot) based on the results for set C. Observational determinations by (Liu et al. 2011) for a large sample of SDSS galaxies are shown with black (gray) crosses for distances from the host up to 150 kpc (250 kpc). The black arrows show how the the occurrence of MC-sized satellites change when the search radii goes from 150 kpc to 250 kpc from the host.

lar to the MCs (Boylan-Kolchin et al. 2010; Busha et al. 2011).

5. DISCUSSION

5.1. Robustness and model uncertainties of the stellar-to-(sub)halo mass relations

The main result from Section 3 is that both the inferred central-halo and satellite-subhalo mass relations do not change for all the combinations of data sets we explored. In other words, these relations seem to be determined robustly, no matter whether only the central/satellite GSMFs (set A) or whether only the total GSMF and the 2PCFs (set B) or whether all of these data (set C) are used. The results confirm what is expected: the GSMFs of central and satellites galaxies are well connected with the 2PCFs and both are part of a general statistical description of the galaxy population. However, it could be that the uncertainties around the mass relations depend on the set of observables used. In particular, we expect that the uncertainties should be smaller when all the observational data are used to constrain the model.

From the results of the MCMC search over 1.5×10^6 models we can identify at each (sub)halo mass the average M_* and its standard deviation. The average stellar masses for a given (sub)halo mass are indistinguishable to those given by the average stellar-to-(sub)halo mass relations constructed with the best fit parameters obtained with the MCMC method. The standard deviations can be interpreted then as the 1σ model-fit uncertainty around these relations (see also More et al. 2011). This uncertainty is due to (i) the inability of the proposed stellar-to-(sub)halo mass relations (Eqs. 5) to reproduce jointly the observational data, and (ii) the observational errors in these data. The dark gray areas in Figs. 3 and 7 correspond to the standard deviations for the set C; the much wider light gray areas show the scatter of 0.25 dex

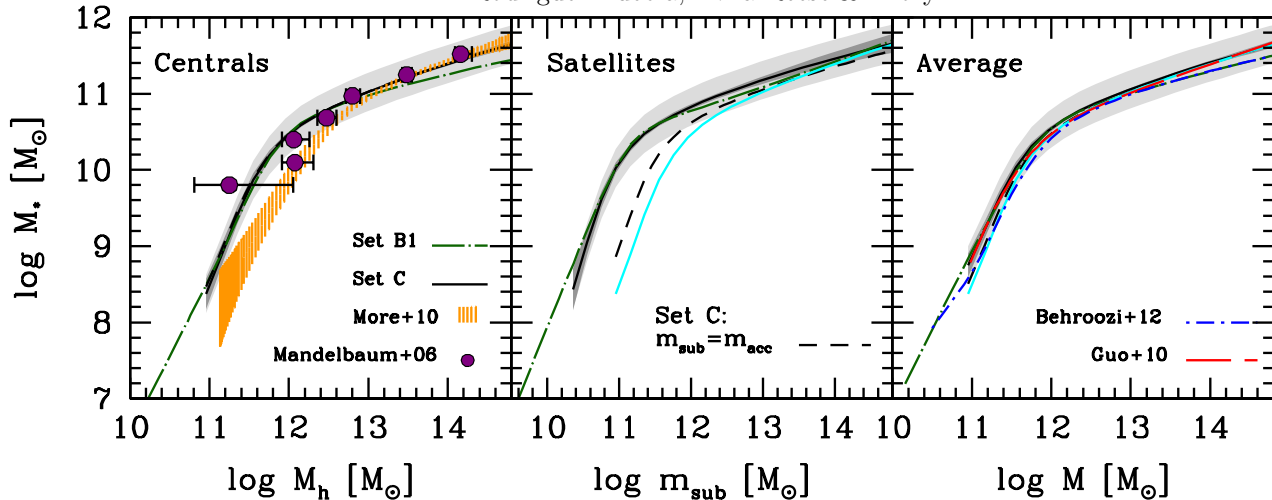


FIG. 7.— Central-halo, satellite-subhalo, and average mass relations for sets C (solid line) and B1 (green dot-dashed line). Short-dashed curves in the medium and right panels are the mass relations when subhalo mass is defined at its accretion time. The systematic uncertainty due to stellar mass determinations is shown with the light-gray shaded area. Gray dashed area indicates the standard deviation of the MCMC model fits in for set C. Filled circles with error bars correspond to the mass relation of central galaxies from the analysis of stacked weak-lensing by Mandelbaum et al. (2006). Orange dashed area indicates the 68% of confidence in the mass relation of central galaxies using the kinematics of satellites (More et al. 2011). Abundance matching results reported in Behroozi & Conroy (2012), and Guo et al. (2010) are plotted with the blue dot-short-dashed and the red long-dashed lines. For comparison we have plotted with the cyan solid lines in the middle and right panels the central-halo mass relations for set C. Observe how in the middle panel the SSMR for the subhalo mass defined at the accretion time lies above the CHMR by a factor of ~ 3 , while in the right panel the nominal average mass relation at the accretion time is a factor of ~ 1.25 higher than the CHMR.

attributed to the systematic uncertainty in the determination of the stellar mass (Behroozi, Conroy & Wechsler 2010).

How do the model-fit uncertainties in the stellar-to-(sub)halo mass relations for set C compare with the other sets? To our surprise, the uncertainties in sets A, B, and B1 are as small as for set C. Actually, the uncertainties are smaller than the intrinsic scatter between galaxy and halo mass at least for halo masses larger than $\sim 10^{11} M_{\odot}$. Lower panels of Fig. 3 show the MCMC standard deviations as a function of (sub)halo mass for all the sets studied here. If any, the major differences are for the uncertainties in the SSMR: they become large at large subhalo masses and are larger for set A (and B1) and smaller for set C. At the smallest (sub)halo masses the model uncertainties for all the sets increase significantly (but yet below the systematic uncertainty of 0.25 dex). This is related to the larger observational errors at smaller stellar masses both for the GSMFs, in particular the one for satellites, and the projected 2PCFs. The small model-fit uncertainties obtained in the determination of the central-halo and satellite-subhalo mass relations through our model again lead us to conclude that these determinations are robust.

How do the stellar-to-(sub)halo mass relations compare with previous work? The most direct (but highly uncertain) methods to infer the halo masses of galaxies for large samples of objects are through weak lensing and satellite kinematics. In the left panel of Fig. 7, we reproduce the results for *central* galaxies of $\langle \log(M_*) \rangle$ as a function of M_h by using stacked satellite kinematics (More et al. 2011, Dr. S. More kindly provided us the data in electronic form) and of $\langle M_h \rangle$ as a function of M_* by using stacked weak lensing analysis⁴

(Mandelbaum et al. 2006). The latter authors inferred the CHMR separated into late- and early-type galaxies, $\langle M_h \rangle_l(M_*)$ and $\langle M_h \rangle_e(M_*)$, respectively. We compute the average $\langle M_h \rangle(M_*)$ relation for all central galaxies as

$$\langle M_h \rangle(M_*) = f_l(M_*) \langle M_h \rangle_l(M_*) + f_e(M_*) \langle M_h \rangle_e(M_*), \quad (29)$$

where $f_l(M_*)$ and $f_e(M_*)$ are the fraction of late- and early-type galaxies of stellar masses M_* in the sample. Note also that for the More et al. (2011) and Mandelbaum et al. (2006) results, small corrections in M_h were applied in order to pass to our definition of virial mass, as well as in M_* to be consistent with the Chabrier (2003) IMF adopted here.

As seen in Fig. 7, the Mandelbaum et al. (2006), weak-lensing determinations are consistent with our CHMR. However if one takes into account that their dependence of $\langle M_h \rangle$ on M_* would be flatter at high masses in case it is deduced from the inverse relation (see footnote), then our determination for set C would be steeper. Instead, the results for set B1 would probably be in better agreement with Mandelbaum et al. (2006) at high masses. The More et al. (2011) satellite-kinematics determinations are consistent with our results for masses larger than $M_h \sim 4 \times 10^{12} M_{\odot}$, but at smaller masses their amplitude can be 2-3 times lower. This discrepancy between satellite kinematics and other methods has been noted previously (e.g., More et al. 2011; Skibba et al. 2011; Rodríguez-Puebla et al. 2011).

In the right panels of Fig. 7 we compare the average stellar-to-halo mass relation (Eq. 18) obtained for set C with those of Guo et al. (2010) (red long-dashed curve) and by Behroozi, Wechsler & Conroy (2012) (blue dot-dashed curve). These authors obtained their relations by matching the abundances of all galaxies to abundances

⁴ As widely discussed in Behroozi, Conroy & Wechsler (2010), due to the scatter, the inferences are slightly different depending

on whether M_* is constrained as a function of M_h or as the inverse. As these authors show the main difference is at the high-mass end.

of halos plus subhalos. In general, our average mass relation is consistent with these previous global AMT results, though a direct comparison might not be fair, because we do not assume that the mass relations for centrals–halos and satellite–subhalos are the same. Also, the definition of subhalo mass used here (at the time of observation) is different to the one used in the above papers, who define it at the time of accretion. Hence, we also plot our SSMR for the subhalo mass defined at the accretion time in Fig. 7 (dashed curve in the central panel, set C) and the corresponding average mass relation (dashed curve in the right panel). The nominal SSMR is close but not equal to the present-day CHMR. We found that the nominal SSMR lies above the CHMR at most by a factor of ~ 3 , while the nominal average mass relation is a factor of ~ 1.25 higher than the CHMR, see also Watson & Conroy (2013). To establish the former relation, one should know how the CHMR (at the accretion time, the satellite is yet a central galaxy and the subhalo is a distinct halo) changes with time, and how the satellite mass evolved since the accretion. Assuming that the CHMR is the same at all epochs leads to the nominal SSMR to be equal to the CHMR (RDA12). The fact that we find both relations to be close (but not equal) implies then that the galaxy–halo connection changes only little with time. This seems to be also the situation in the cosmological simulations (Simha et al. 2012; De Rossi et al. 2013).

For set B1, which uses the BGD08 GSMF, the CHMR changes slightly its slope at low masses, while the SSMR becomes systematically shallower than in the case of set C. This is because the BGD08 GSMF becomes steeper at lower masses. However, when the density-weighted average is calculated, the slope change seen for the centrals is almost smeared out. For the Behroozi, Wechsler & Conroy (2012) total (average) mass relation the slope change is present, presumably because the contribution of the satellite-subhalo mass relation is not taken into account. On the other hand, if we use the subhalo mass at the accretion time instead that at the observation time, then the smearing-out of the slope change is less evident.

5.2. The satellite-subhalo mass relation at the low-mass end

An interesting question is how to extend the GSMFs and stellar-to-(sub)halo mass relations towards low masses, since most potential issues with the Λ CDM scenario are happening at small scales. As recently discussed by Boylan-Kolchin, Bullock & Kaplinghat (2012), the Λ CDM scenario can be compatible with the overall abundance of MW satellites, but it predicts subhalos that are too massive (or too concentrated) compared to dynamical observations of the brightest dwarf spheroidal (dSph) satellites. This can be visualized using the dSph stellar mass vs. subhalo maximum circular velocity (or mass) diagram, comparing the observations for the bright MW dSphs with extrapolations of *total* (centrals+satellites) abundance matching results to low masses. For a given M_* , the MW dSphs have subhalo circular velocities (or masses) much larger (by $\sim 1.5 - 2$ dex in mass) than the extrapolated AMT results.

Our model has the advantage that it allows to constrain the CHMR and the SSMR separately (Fig. 3).

The extrapolation of the latter only is what actually should be used for comparison with the MW satellites. RDA12 show that if the faint-end extrapolation of the GSMF is as steep as -1.6 (BGD08; Drory et al. 2009) and is completely dominated by satellite galaxies, then the Λ CDM subhalo masses are consistent with the subhalo masses of the observed MW dSphs. Here, masses are defined at the estimated tidal radii of the dwarf satellites (see Fig. 2 in RDA12 and references therein). By using our model, we are able to decompose the BGD08 GSMF into satellites and centrals (set B1; Fig. 1). The faint-end slope of the satellite GSMF (down to $\sim 2.5 \times 10^7 M_\odot$) indeed resembles the total mass function, *but satellites do not dominate over centrals*. Therefore, the inferred SSMR gives still too large subhalo masses (by 0.3–0.4 dex) as compared with the tidal masses of the MW dwarfs. We should note that in set B1, the Y12 projected 2PCFs are used, and for stellar masses smaller than reported in Y12 ($\sim 1 \times 10^9 M_\odot$), no projected 2PCF constraints are applied. There are some hints that the projected 2PCFs of galaxies at small distances (one-halo term, where satellites dominate) are steeper than those measured in YMB09, especially for the smallest galaxies (Li & White 2009). If this is the case, then we can easily show that the satellites become more abundant in the GSMF and the SSMR is flatter at low masses, leading to a better agreement with the inferred tidal (subhalo) masses for the MW dSph satellites.

5.3. Interpreting the bump of the GSMF

Several interpretations of the shape of the total GSMF have been offered in the literature (Baldry, Glazebrook & Driver 2008; Drory et al. 2009; Li & White 2009; Bolzonella et al. 2010; Pozzetti et al. 2010). In this section we will focus on interpreting the shape of the GSMF using arguments based on the occupation statistics of galaxies within halos. Looking at Fig. 5, it becomes apparent that as halo mass increases, the likelihood of finding at least one satellite with a stellar mass *similar* to that of the central galaxy increases rapidly. Also, the stellar mass range covered by the satellite population is narrower and closer to that of the central as halo mass increases. Assuming that these features of the satellite population mass distribution are robust and have been in place since the assembly of the central, it follows that the central’s probability of growing by accreting large (compared to itself) satellites was largest in high-mass halos that today occupy the bump and high-mass end of the mass function.

6. CONCLUSIONS

An statistical model that combines the AMT with the HOD and CSMF formalisms is presented. The model allows to constrain the central-halo and satellite-subhalo mass relations (CHMR and SSMR) separately, as well as the satellite CSMFs inside the halos. The Λ CDM halo mass function and subhalo conditional mass functions were used as input. From the observational point of view, the model works with the total GSMF and its decomposition into centrals and satellites, and the 2PCFs. Therefore, the observations used to constrain the model can be different combinations of data: either the central/satellite GSMFs (from YMB09; set A), or the total GSMF (from YMB09 or BGD08) and the Y12 projected

2PCFs (sets B and B1), or all the data, i.e., the GSMFs of centrals and satellites and the projected 2PCFs (set C). Our aim was to explore how sensitive are the determinations of the mass relations and their uncertainties to the different data set used to constrain the model, as well as to test the overall consistency of the observations with the Λ CDM halo/subhalo mass functions. Related to the latter, we explored model predictions regarding some satellite number distributions. The main conclusions we arrive at are:

- The constrained parameters of the CHMR and SSMR are almost identical for all sets of data, showing that these relations (and therefore, also the satellite CSMFs) are robust with respect to what combinations of data are used to constrain the model. To our surprise, even the model-fit uncertainties in the constrained stellar-to-(sub)halo mass relations are very similar for the different combinations of data sets, including the one where all the data are used (set C). These uncertainties are smaller than the assumed intrinsic scatters (0.173 dex) for $M_h \gtrsim 10^{11} M_\odot$, and of that order for smaller masses where the observational determinations of the GSMFs and projected 2PCFs have larger errors.

- For set A, the projected 2PCFs are predictions, while for set B (and B1), the GSMF decomposition into centrals and satellites are predictions of the model. In each case, these predictions agree very well with the observations. This shows that matching central/satellite and (sub)halo *abundances* (set A) is equivalent to matching central/satellite and (sub)halo *occupational numbers*, in which case the 2PCFs are necessary (sets B, B1), and vice versa. In both cases, the CHMR and SSMR are intermediate relations. The key novelty in our model is that both relations are constrained separately instead of being assumed equal. Our results show also that the satellite/central GSMF is tightly connected to the spatial clustering of the population, both at the level of the one- and two-halo terms, as well as with the satellite mass functions inside the halos.

- For set C, neither the projected 2PCFs nor the GSMF decomposition are predictions, instead observational determinations of these functions are used to constrain the model. This allows us to leave the widths of the intrinsic scatter around the CHMR and SSMR (assumed independent of mass and log-normally distributed) as free parameters. We obtain $\sigma_c = 0.168 \pm 0.051$ dex and $\sigma_s = 0.172 \pm 0.057$ dex. For centrals, our result confirms previous estimates, and for satellites we find that the intrinsic scatter is almost the same as for centrals.

- The satellite-subhalo mass relation, where subhalo masses are defined at the observation time, is not equal to the central-halo relation. For the former, the stellar mass scales as $M_h^{2.5}$ at the low mass-end and as $M_h^{1.7}$ at the high-mass end (set C), while for the latter, these scalings go as $M_* \propto M_h^{2.9}$ and $M_h^{1.7}$, respectively. This difference is mainly due to the fact that subhalos lose mass (60-65%) due to tidal stripping. When m_{sub} is defined at the accretion time, the nominal SSMR is actually close to the CHMR but again not equal. The SSMR lies above the CHMR at most by a factor of ~ 3 , while the average mass relation is a factor of ~ 1.25 higher than the CHMR, implying that the CHMR likely changes lit-

tle with time.

- In set B1, we use the BGD08 total GSMF, which extends to masses as low as $\log(M_*/M_\odot)=7.4$. This function is steeper at the low- M_* end and decays faster at the highest masses than the YMB09 GSMF. Therefore, the CHMR and SSMR are slightly different to those in set B. In particular, the lowest masses show a slight flattening as compared to results of set B. For the satellites, if extrapolated to even lower masses, this implies smaller subhalo masses for a given stellar mass than usually obtained from the standard AMT. This is diminishing the potential problem of too massive Λ CDM subhalos for the bright MW dSphs.

Our model allows us to infer in a natural way any statistical distribution for the central and satellite galaxy populations, as for example the satellite CSMF and the mass distributions and probabilities of particular subpopulations of satellites as a function of halo mass. The obtained satellite CSMFs in different halo mass bins agree very well with those inferred from the SDSS halo-based galaxy groups in YMB09. Moreover, we have explored in particular two interesting statistics related to well-posed astronomical problems, (1) the distribution of the stellar mass gap between the central and the most-massive satellite galaxy as a function of halo mass, and (2) the probabilities for MW-like halos to have N_{MC} MC-sized satellites. Our conclusions regarding these questions are:

- (1) With decreasing halo mass, the mass distribution of the most massive satellite as compared to the the distribution of the central galaxy become more different and shifted to lower masses. This shows that the central is a statistically exceptional galaxy in the halo (group). For masses larger than $M_h \sim 3 \times 10^{13} M_\odot$, the differences become smaller but even in this case only $\sim 15\%$ of halos seem to have the most massive satellite statistically indistinguishable from the central one, which implies that the latter could be a mere statistical realization of the massive-end of the satellite CSMF instead of realization of a different galaxy.

- (2) For the range of halo masses in question for the MW, we find that the probabilities to have N_{MC} MC-sized satellites are in good agreement with the observational determinations by Liu et al. (2011). A MW-halo mass of $\lesssim 2 \times 10^{12} M_\odot$ would agree better with the observational determinations for two MC-sized satellites ($N_{\text{MC}} = 2$). When excluding the cases that satellites are larger than the LMC, the probabilities become even lower: $< 2.2\%$ for $M_h = 2 \times 10^{12} M_\odot$.

We conclude that the semi-empirical results we obtain here, both for the central-halo and satellite-subhalo mass relations and their intrinsic scatters, are quite robust and imply full consistency of the Λ CDM halo and subhalo populations with several statistical distributions of the observed populations of central and satellite galaxies down to $M_* \sim 10^9 M_\odot$.

We thank the Referee, David Weinberg, for a constructive report that helped to improve the paper. A. R-P acknowledges a graduate student fellowship provided by CONACyT. N. D. and V. A. acknowledge CONACyT grants 128556 and 167332.

REFERENCES

- Abbas U., Sheth R. K., 2006, *MNRAS*, 372, 1749
 Baldry I. K., Glazebrook K., Driver S. P., 2008, *MNRAS*, 388, 945
 Behroozi P. S., Conroy C., Wechsler R. H., 2010, *ApJ*, 717, 379
 Behroozi P. S., Wechsler R. H., Conroy C., 2012, *ArXiv e-prints*
 Berlind A. A., Weinberg D. H., 2002, *ApJ*, 575, 587
 Bolzonella M. et al., 2010, *A&A*, 524, A76
 Boylan-Kolchin M., Bullock J. S., Kaplinghat M., 2012, *MNRAS*, 422, 1203
 Boylan-Kolchin M., Springel V., White S. D. M., Jenkins A., 2010, *MNRAS*, 406, 896
 Bryan G. L., Norman M. L., 1998, *ApJ*, 495, 80
 Busha M. T., Marshall P. J., Wechsler R. H., Klypin A., Primack J., 2011, *ApJ*, 743, 40
 Cacciato M., van den Bosch F. C., More S., Li R., Mo H. J., Yang X., 2009, *MNRAS*, 394, 929
 Chabrier G., 2003, *PASP*, 115, 763
 Conroy C. et al., 2007, *ApJ*, 654, 153
 Conroy C., Wechsler R. H., 2009, *ApJ*, 696, 620
 Conroy C., Wechsler R. H., Kravtsov A. V., 2006, *ApJ*, 647, 201
 Cooray A., 2006, *MNRAS*, 365, 842
 Cooray A., Sheth R., 2002, *PhR*, 372, 1
 De Rossi M. E., Avila-Reese V., Tissera P., Gonzalez-Samaniego A., Pedroza S., 2013, submitted
 Drory N. et al., 2009, *ApJ*, 707, 1595
 Dunkley J., Bucher M., Ferreira P. G., Moodley K., Skordis C., 2005, *MNRAS*, 356, 925
 Gao L., Frenk C. S., Boylan-Kolchin M., Jenkins A., Springel V., White S. D. M., 2011, *MNRAS*, 410, 2309
 Giocoli C., Tormen G., van den Bosch F. C., 2008, *MNRAS*, 386, 2135
 Guo Q., White S., Li C., Boylan-Kolchin M., 2010, *MNRAS*, 404, 1111
 Hansen S. M., Sheldon E. S., Wechsler R. H., Koester B. P., 2009, *ApJ*, 699, 1333
 Hearin A. P., Zentner A. R., Berlind A. A., Newman J. A., 2012, *ArXiv e-prints*
 James P. A., Ivory C. F., 2011, *MNRAS*, 411, 495
 Kravtsov A. V., Berlind A. A., Wechsler R. H., Klypin A. A., Gottlöber S., Allgood B., Primack J. R., 2004, *ApJ*, 609, 35
 Leauthaud A., Tinker J., Behroozi P. S., Busha M. T., Wechsler R. H., 2011, *ApJ*, 738, 45
 Leauthaud A. et al., 2012, *ApJ*, 744, 159
 Li C., White S. D. M., 2009, *MNRAS*, 398, 2177
 Liu L., Gerke B. F., Wechsler R. H., Behroozi P. S., Busha M. T., 2011, *ApJ*, 733, 62
 Mandelbaum R., Seljak U., Hirata C. M., 2008, *JCAP*, 8, 6
 Mandelbaum R., Seljak U., Kauffmann G., Hirata C. M., Brinkmann J., 2006, *MNRAS*, 368, 715
 Milosavljević M., Miller C. J., Furlanetto S. R., Cooray A., 2006, *ApJ*, 637, L9
 More S., 2012, *ApJ*, 761, 127
 More S., van den Bosch F. C., Cacciato M., Mo H. J., Yang X., Li R., 2009, *MNRAS*, 392, 801
 More S., van den Bosch F. C., Cacciato M., Skibba R., Mo H. J., Yang X., 2011, *MNRAS*, 410, 210
 Moster B. P., Somerville R. S., Maulbetsch C., van den Bosch F. C., Macciò A. V., Naab T., Oser L., 2010, *ApJ*, 710, 903
 Muñoz-Cuartas J. C., Macciò A. V., Gottlöber S., Dutton A. A., 2011, *MNRAS*, 411, 584
 Neistein E., Li C., Khochfar S., Weinmann S. M., Shankar F., Boylan-Kolchin M., 2011, *MNRAS*, 416, 1486
 Papastergis E., Cattaneo A., Huang S., Giovanelli R., Haynes M. P., 2012, *ApJ*, 759, 138
 Peacock J. A., Smith R. E., 2000, *MNRAS*, 318, 1144
 Peebles P. J. E., 1980, *The large-scale structure of the universe*
 Pozzetti L. et al., 2010, *A&A*, 523, A13
 Press W. H., Teukolsky S. A., Vetterling W. T., Flannery B. P., 1992, *Numerical recipes in C. The art of scientific computing*, Press, W. H., Teukolsky, S. A., Vetterling, W. T., & Flannery, B. P., ed.
 Reddick R. M., Wechsler R. H., Tinker J. L., Behroozi P. S., 2012, *ArXiv e-prints*
 Rodríguez-Puebla A., Avila-Reese V., Firmani C., Colín P., 2011, *RMxAA*, 47, 235
 Rodríguez-Puebla A., Drory N., Avila-Reese V., 2012, *ApJ*, 756, 2
 Schechter P., 1976, *ApJ*, 203, 297
 Schulz A. E., Mandelbaum R., Padmanabhan N., 2010, *MNRAS*, 408, 1463
 Seljak U., 2000, *MNRAS*, 318, 203
 Shankar F., Lapi A., Salucci P., De Zotti G., Danese L., 2006, *ApJ*, 643, 14
 Sheth R. K., Hui L., Diaferio A., Scoccimarro R., 2001, *MNRAS*, 325, 1288
 Sheth R. K., Mo H. J., Tormen G., 2001, *MNRAS*, 323, 1
 Simha V., Weinberg D. H., Davé R., Fardal M., Katz N., Oppenheimer B. D., 2012, *MNRAS*, 423, 3458
 Skibba R. A., van den Bosch F. C., Yang X., More S., Mo H., Fontanot F., 2011, *MNRAS*, 410, 417
 Smith R. E. et al., 2003, *MNRAS*, 341, 1311
 Tinker J., Kravtsov A. V., Klypin A., Abazajian K., Warren M., Yepes G., Gottlöber S., Holz D. E., 2008a, *ApJ*, 688, 709
 Tinker J. L., Conroy C., Norberg P., Patiri S. G., Weinberg D. H., Warren M. S., 2008b, *ApJ*, 686, 53
 Tinker J. L., Weinberg D. H., Zheng Z., Zehavi I., 2005, *ApJ*, 631, 41
 Tremaine S. D., Richstone D. O., 1977, *ApJ*, 212, 311
 Vale A., Ostriker J. P., 2004, *MNRAS*, 353, 189
 Vale A., Ostriker J. P., 2008, *MNRAS*, 383, 355
 Wake D. A., Franx M., van Dokkum P. G., 2012, *ArXiv e-prints*
 Watson D. F., Berlind A. A., McBride C. K., Hogg D. W., Jiang T., 2012, *ApJ*, 749, 83
 Watson D. F., Berlind A. A., Zentner A. R., 2011, *ApJ*, 738, 22
 Watson D. F., Berlind A. A., Zentner A. R., 2012, *ApJ*, 754, 90
 Watson D. F., Conroy C., 2013, *ArXiv e-prints*
 Weinberg D. H., Colombi S., Davé R., Katz N., 2008, *ApJ*, 678, 6
 Wetzel A. R., Tinker J. L., Conroy C., 2012, *MNRAS*, 424, 232
 Wojtak R., Mamon G. A., 2013, *MNRAS*, 428, 2407
 Yang X., Mo H. J., van den Bosch F. C., 2003, *MNRAS*, 339, 1057
 Yang X., Mo H. J., van den Bosch F. C., 2008, *ApJ*, 676, 248
 Yang X., Mo H. J., van den Bosch F. C., 2009a, *ApJ*, 695, 900
 Yang X., Mo H. J., van den Bosch F. C., 2009b, *ApJ*, 693, 830
 Yang X., Mo H. J., van den Bosch F. C., Pasquali A., Li C., Barden M., 2007, *ApJ*, 671, 153
 Yang X., Mo H. J., van den Bosch F. C., Zhang Y., Han J., 2012, *ApJ*, 752, 41
 Yoo J., Weinberg D. H., Tinker J. L., Zheng Z., Warren M. S., 2009, *ApJ*, 698, 967
 Zavala J., Avila-Reese V., Firmani C., Boylan-Kolchin M., 2012, *MNRAS*, 427, 1503
 Zehavi I. et al., 2011, *ApJ*, 736, 59
 Zehavi I. et al., 2005, *ApJ*, 630, 1
 Zheng Z. et al., 2005, *ApJ*, 633, 791
 Zheng Z., Coil A. L., Zehavi I., 2007, *ApJ*, 667, 760

APPENDIX

THE FITTING PROCEDURE

From the fit to the data, we constrain the ten free parameters of model by maximizing the likelihood function $\mathcal{L} \propto \exp(-\chi^2/2)$. Table 1 lists the different combination of observational constrains used in this paper.

For each GSMF, the χ^2 's are defined as:

$$\chi^2(\phi_{\text{tot,cen,sat}}^{\text{author}}) = \frac{1}{N_{\text{bin}}} \sum_{i=1}^{N_{\text{bin}}} \left(\frac{\phi_{g,\text{model}}^i - \phi_{g,\text{obs}}^i}{\sigma_{\text{obs}}^i} \right)^2, \quad (\text{A1})$$

where N_{bin} is the number of bins in the total/central/satellite GSMF reported for each author with an i th value of $\phi_{g,\text{obs}}^i$ and an error of σ_{obs}^i . The i th value of the total/central/satellite GSMF computed in the model is denoted as $\phi_{g,\text{model}}^i$.

For the Yang et al. (2012) projected 2PCFs, the χ^2 is defined as:

$$\chi^2(w_{\text{p,bin}}^{\text{Y11}}) = \frac{1}{N_{\text{s,bin}} N_{\text{r,bin}}} \sum_{i=1}^{N_{\text{s,bin}}} \sum_{j=1}^{N_{\text{r,bin}}} \left(\frac{w_{\text{p,model}}^{i,j} - w_{\text{p,obs}}^{i,j}}{\sigma_{\text{obs}}^{i,j}} \right)^2, \quad (\text{A2})$$

where $N_{\text{s,bin}}$ is the number of stellar mass bins, $N_{\text{r,bin}}$ denotes the number of bins in the 2PCF, $w_{\text{p,obs}}^{i,j}$ ($w_{\text{p,model}}^{i,j}$) is the amplitude of the observed (modeled) 2PCF in the j th projected distance bin of the i th stellar mass bin.

First, we find the set of parameters, $\mathbf{a} = (a_1, \dots, a_n)$, that minimizes χ^2 using the Powell's directions set method in multi-dimensions, Press et al. (1992). Then, the resulting set of parameters is used as the starting point to sample the parameter space with the MCMC method. In most of our cases $n = 10$. We also need to specify for each parameter a proposed distribution, which generates the candidate for sampling the parameter space. We assume that each proposed distribution is Gaussian distributed. The standard deviation for each parameter, $\sigma(a_i)$, is calculated from the covariance matrix. The covariance matrix or error matrix of \mathbf{a} is defined as the inverse of the $n \times n$ matrix $\alpha = \epsilon^{-1}$, computed according to

$$\alpha_{kl} = \frac{1}{2} \frac{\partial^2 \chi^2(\mathbf{a})}{\partial a_k \partial a_l}. \quad (\text{A3})$$

Therefore, the standard deviations in the parameters correspond to the square roots of the terms in its diagonal, i.e., $\sigma(a_i) = \sqrt{\epsilon_{ii}}$. We consider these numbers as our best initial guess for the diagonal covariance matrix of the model parameters. Then the covariance matrix for the proposed matrix is computed according to the formula given in (Dunkley et al. 2005); $\epsilon_{ii}^{\text{p}} = \frac{2.4^2}{n} \epsilon_{ii}$, with n the number of parameters to be fitted.

Using these results, we sample a first chain with 100,000 models, from which we compute the diagonal of the covariance matrix, ϵ_{ii}^{c} . If the ratio of each prior, $\sqrt{\epsilon_{ii}}$, to each element of the resulting diagonal covariance matrix, $\sqrt{\epsilon_{ii}^{\text{c}}}$, lies in the range $0.8 \leq \sqrt{\epsilon_{ii}/\epsilon_{ii}^{\text{c}}} \leq 1.2$, then we initialize a second chain with 1.5×10^6 elements for the model analysis; else, we repeat the procedure j -times until the ratio of the covariances of the previous chain with the last one reaches the condition $0.8 \leq \sqrt{\epsilon_{ii}^{j-1}/\epsilon_{ii}^j} \leq 1.2$, that is to say, until there is not a sufficiently significant improvement in the standard deviations of the model parameters. The j -covariance matrix for the proposed distribution is given by $\epsilon_{ii}^{\text{p},j} = \frac{2.4^2}{n} \epsilon_{ii}^j$. Then, we run a last chain with 1.5×10^6 elements for the model analysis. This procedure usually takes one or two iterations. For all the chains, we find a convergence ratio in each parameter lower than 0.01 (Dunkley et al. 2005).